17. J. J. Zhu, J. A. Esteban, Y. Hayashi, R. Malinow, *Nat. Neurosci.* **3**, 1098 (2000).
18. S. Kim *et al.*, *Nat. Neurosci.* **9**, 1294 (2006).
19. J. Ko *et al.*, *Neuron* **50**, 233 (2006).
20. M. W. Linhoff *et al.*, *Neuron* **61**, 734 (2009).
21. H. Takahashi *et al.*, *Neuron* **69**, 287 (2011).
22. C. Rosenmund, J. D. Clements, G. L. Westbrook, *Science* **262**, 754 (1993).
23. H. Y. Sun, L. E. Dobrunz, *J. Neurosci.* **26**, 10796 (2006).
24. H. Y. Sun, A. F. Bartley, L. E. Dobrunz, *J. Neurophysiol.* **101**, 1043 (2009).
25. K. A. Buchanan *et al.*, *Neuron* **75**, 451 (2012).
26. H. Y. Sun, S. A. Lyons, L. E. Dobrunz, *J. Physiol.* **568**, 815 (2005).
27. T. Klausberger *et al.*, *Nature* **421**, 844 (2003).
28. G. Buzsáki, *Neuroscience* **31**, 551 (1989).
29. J. Larson, D. Wong, G. Lynch, *Brain Res.* **368**, 347 (1986).
30. C. H. Vanderwolf, *Electroencephalogr. Clin. Neurophysiol.* **26**, 407 (1969).

Acknowledgments: We thank M. Scanziani, P. Scheiffele, and members of the Ghosh lab for suggestions and comments on the manuscript; J. de Wit for generating the Elfn1-GFP construct; and M. Macias, C. Sanchez, and E. Kang for help with virus and protein production. This work was supported by NIH grant R01NS067216 and the Gatsby Charitable Foundation.

Supplementary Materials
www.sciencemag.org/cgi/content/full/science.1222482/DC1
Materials and Methods
Supplementary Text
Figs. S1 to S8
References (*31*–*34*)

27 March 2012; accepted 11 September 2012
Published online 4 October 2012;
10.1126/science.1222482

Oxytocin/Vasopressin-Related Peptides Have an Ancient Role in Reproductive Behavior

Jennifer L. Garrison, Evan Z. Macosko, Samantha Bernstein, Navin Pokala, Dirk R. Albrecht, Cornelia I. Bargmann

Many biological functions are conserved, but the extent to which conservation applies to integrative behaviors is unknown. Vasopressin and oxytocin neuropeptides are strongly implicated in mammalian reproductive and social behaviors, yet rodent loss-of-function mutants have relatively subtle behavioral defects. Here we identify an oxytocin/vasopressin-like signaling system in *Caenorhabditis elegans*, consisting of a peptide and two receptors that are expressed in sexually dimorphic patterns. Males lacking the peptide or its receptors perform poorly in reproductive behaviors, including mate search, mate recognition, and mating, but other sensorimotor behaviors are intact. Quantitative analysis indicates that mating motor patterns are fragmented and inefficient in mutants, suggesting that oxytocin/vasopressin peptides increase the coherence of mating behaviors. These results indicate that conserved molecules coordinate diverse behavioral motifs in reproductive behavior.

Animal behaviors such as mating, feeding, or foraging typically involve combinations of simpler actions and motor patterns that develop over different time scales. In the case of reproductive behavior, neuropeptide signaling through oxytocin and vasopressin peptides may provide a global organizing role. The mammalian hypothalamic neuropeptide oxytocin, released during birth, stimulates maternal behaviors as well as uterine contractions and lactation, and the related peptide vasopressin is linked to male-typical behaviors in rodents and fish, in addition to its role in fluid homeostasis (*1*). Similarly, administration of the oxytocin/vasopressin-related peptide conopressin to leeches stimulates reproductive behaviors and mating-related neuronal activity (*2*). A more general role for oxytocin in social behaviors is suggested by the social amnesia of oxytocin mutant mice (*3*) and by altered social decision-making in humans after oxytocin administration (*4*). However, mammalian oxytocin and vasopressin mutants have subtle behavioral defects relative to the potency of the administered peptides (*5*). To define the role of these neuropeptides in endogenous reproductive behaviors, we here address their function through genetic analysis of an oxytocin/vasopressin-related neuropeptide in the nematode *Caenorhabditis elegans*.

Through homology searches, we identified a gene in *C. elegans* with similarity to mammalian vasopressin and oxytocin (*ntc-1*; Fig. 1, A and B, and fig. S1). To determine whether this gene generates an authentic neuropeptide, we isolated total neuropeptides from wild-type animals and characterized them by tandem mass

Howard Hughes Medical Institute, Lulu and Anthony Wang Laboratory of Neural Circuits and Behavior, The Rockefeller University, New York, NY 10065, USA.

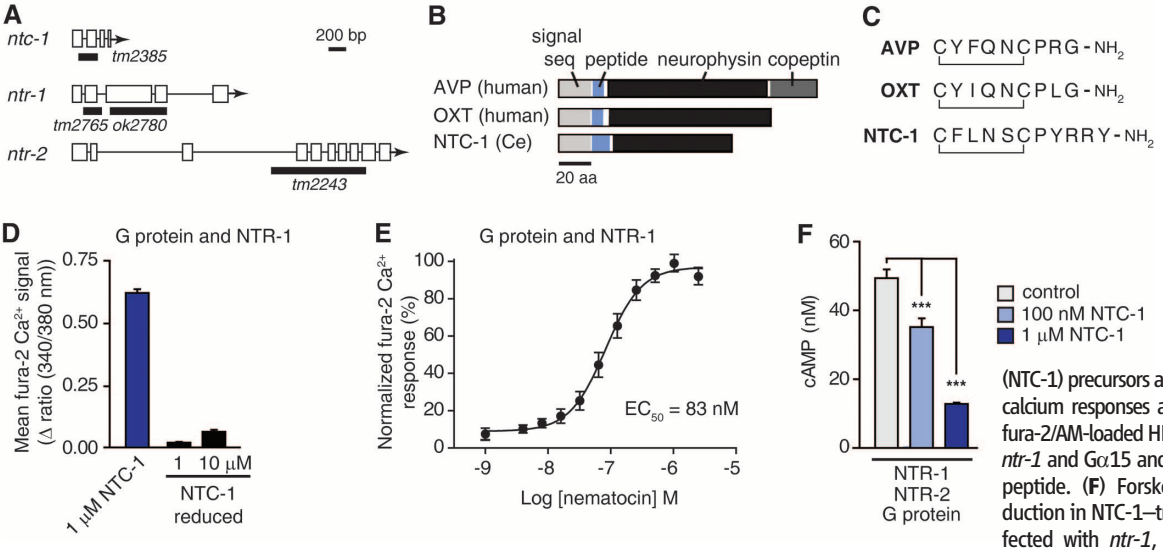

Fig. 1. *ntc-1* encodes an oxytocin/vasopressin-related peptide that signals through receptors encoded by *ntr-1* and *ntr-2*. (**A**) Gene models with deletions in mutant alleles indicated by horizontal black bars (www.wormbase.org). (**B** and **C**) Domain structure and amino acid sequence of vasopressin (AVP), oxytocin (OXT), and nematocin (NTC-1) precursors and peptides. (**D** and **E**) Mean calcium responses and dose-response curves of fura-2/AM-loaded HEK293T cells transfected with *ntr-1* and Gα15 and exposed to synthetic NTC-1 peptide. (**F**) Forskolin-stimulated cAMP production in NTC-1–treated HEK293T cells transfected with *ntr-1*, *ntr-2*, and Gα15. ***$P <$ 0.0001. Error bars in all figures indicate SEM.

spectrometry (*6*), identifying a peptide matching the mass predicted for an 11–amino acid cyclized peptide with an amidated C terminus (Fig. 1C and fig. S2). Fragmentation of this peptide by liquid chromatography–tandem mass spectrometry confirmed the existence of a *C. elegans* neuropeptide, nematocin. The *C. elegans* genome also predicts two genes encoding G protein–coupled receptors related to vertebrate oxytocin and vasopressin receptors, the nematocin receptor (*ntr*) genes (Fig. 1A and figs. S3 and S4). To determine whether these encode nematocin receptors, we expressed *ntr-1* and *ntr-2* cDNAs in HEK293T cells with the promiscuous G protein Gα15 and administered a synthetic cyclized peptide corresponding to nematocin. Cells transfected with *ntr-1* responded to nematocin with calcium transients and a nanomolar median effective concentration (EC_{50}) (Fig. 1, D and E, and fig. S1). Cells transfected with *ntr-2* did not mobilize calcium in response to nematocin, but cells cotransfected with both receptors responded to nematocin with decreases in intracellular cyclic adenosine monophosphate (cAMP), suggesting coupling to a signaling pathway that antagonizes adenylyl cyclase (Fig. 1F and fig. S1) (*7*). Although heterologous expression may not capture all native functions, these results suggest that NTR-1 and NTR-2 can contribute

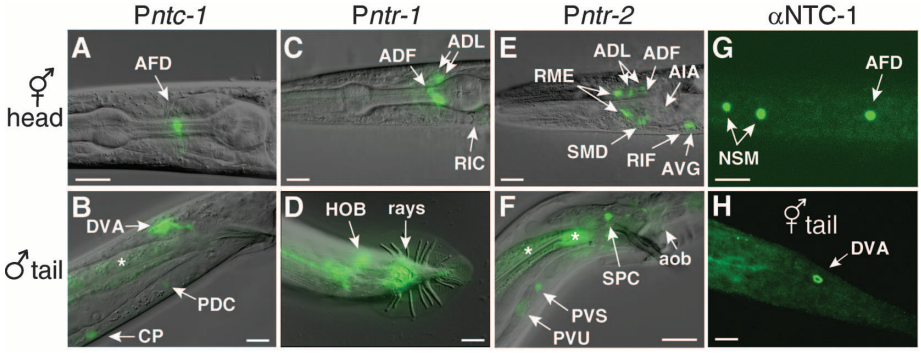

Fig. 2. *ntc-1*, *ntr-1*, and *ntr-2* expression patterns. P, gene promoter fragment used. The upper panels show expression in adult hermaphrodite heads; the lower panels show male [(B), (D), and (F)] and hermaphrodite (H) tails. (**A** to **F**) Expression of *ntc-1*, *ntr-1*, and *ntr-2* reporter genes (table S1). (**G** and **H**) Immunostaining of AFD, NSM, and DVA neurons with antisera to nematocin. White arrows indicate expression in specified neurons. Asterisks mark autofluorescence; scale bars represent 10 μm.

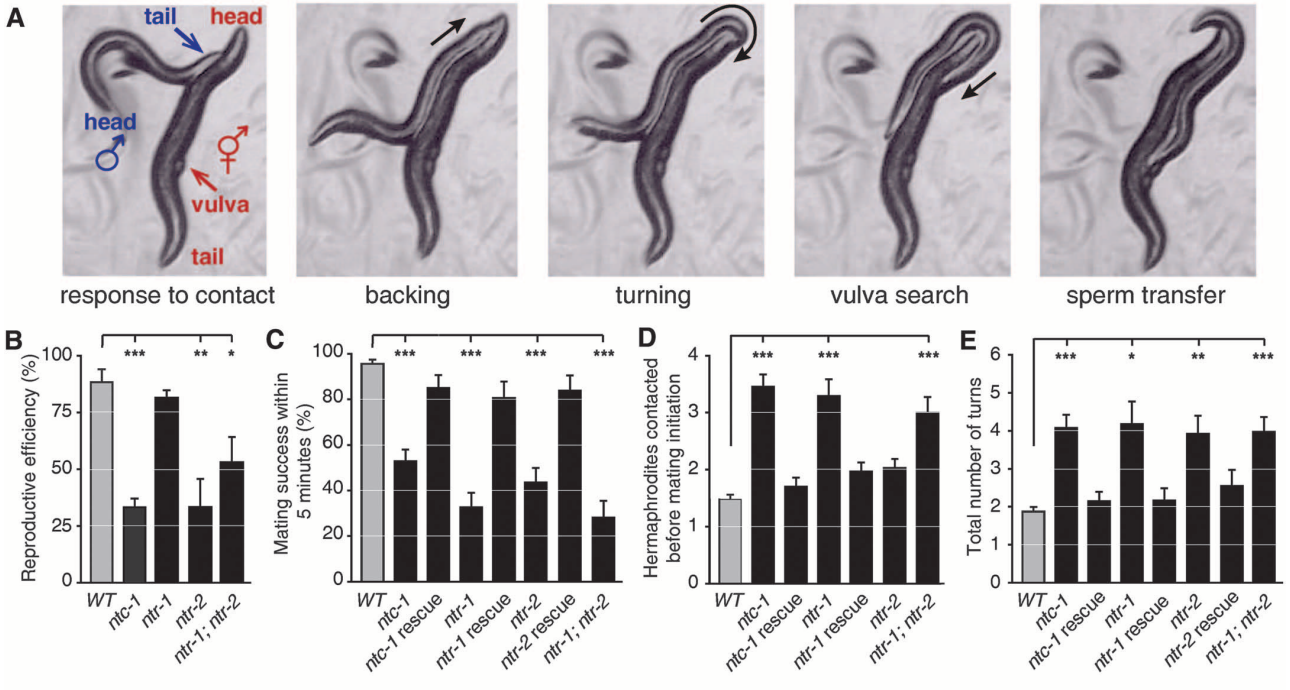

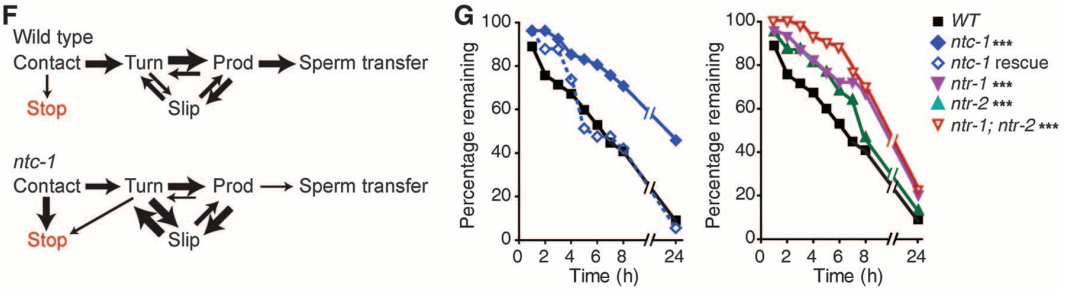

Fig. 3. Nematocin-deficient males exhibit mating defects. (**A**) Steps in male mating behavior. The black arrow notes the direction of male movement. (**B**) Reproductive efficiencies of wild-type (WT, gray bars) and mutant males (black bars) in long-term single-pair mating crosses (no. of cross-progeny/no. of total progeny). (**C**) Percentage of males that successfully transferred sperm within 5 min of first tail contact with a hermaphrodite. (**D**) Mean number of hermaphrodites that a male's tail contacted before he initiated mating. (**E**) Mean total number of turns a male executed around the hermaphrodite's body before locating the vulva. (**F**) Summary of the behavioral transitions in ethograms of male mating behavior (figs. S8 and S9); the arrow width indicates the probability of behavioral transitions. (**G**) Male mate search behavior, measured as the rate at which a single male leaves food in the absence of hermaphrodites (*15*). *$P < 0.01$, **$P < 0.001$, ***$P < 0.0001$.

to nematocin-mediated signaling alone (NTR-1) or as heterodimers (NTR-1/NTR-2).

The expression of nematocin and *ntr* genes was examined by conventional and fosmid-recombineered green fluorescent protein (GFP) reporter genes and additionally with antisera generated against synthetic nematocin (Fig. 2, A to H; figs. S5 and S6; and table S1). *C. elegans* has two sexes, self-fertilizing hermaphrodites that can also mate as females, and cross-fertilizing males (*8*). Both sexes expressed nematocin in the AFD thermosensory neurons, which mediate thermotaxis (*9*), and in the DVA mechanosensory neuron, which regulates locomotion and posture (*10*); and males expressed nematocin in male-specific CP motor neurons that control turning behavior during mating (*11*) (Fig. 2, A and B, and G and H). Both sexes expressed *ntr* receptor reporter genes in partly overlapping sets of head and tail neurons, and males additionally expressed them in male-specific neurons and muscles implicated in mating (Fig. 2, C to F; fig. S6; and table S1): *ntr-1* in hook and tail sensory neurons [HOB, which senses the vulva; and rays 1, 5, 7, and 9, which sense hermaphrodite contact (*12*)] and in spicule protractor muscles, which act during sperm transfer (*13*); and *ntr-2* in the male-specific SPC sensory-motor tail neurons that induce spicule penetration and muscle contraction for sperm transfer (*13*, *14*) and in the male-specific oblique muscles that promote prolonged vulval contact (*14*). The reporter genes rescued all behavioral phenotypes described below, indicating that they are expressed in functionally relevant sites (Fig. 3).

Null mutants for nematocin and the two *ntr* genes were viable and fertile as hermaphrodites, with normal locomotion speed, egg-laying behavior, and numbers of progeny (fig. S7). The males were also viable, but they had reduced mating success: When single males were housed with single mating partners, the number of progeny per male was reduced 2.5-fold in nematocin or *ntr-2* mutants as compared to wild-type males (Fig. 3B). We characterized the male mating defect by quantitative analysis of mating encounters between individual virgin males and hermaphrodite mating partners in a 5-min viewing period, and found that nematocin mutant males were inefficient at multiple mating stages. When placed in a small arena with food and mating partners, a wild-type male typically attempted to mate with the first hermaphrodite that his tail touched, located her vulva after he made one or two turns around her body, and successfully transferred sperm within 5 min (Fig. 3A and C to E, and fig. S8). Nematocin mutant males attempted to mate only after numerous hermaphrodite contacts (Fig. 3D), made more turns around the hermaphrodite before locating the vulva (Fig. 3E), and had difficulty executing turns, maintaining vulval contact, and transferring sperm within the assay period (Fig. 3C and fig. S8). Ethograms showed fragmentation of the mating sequence and repetition of early mating steps in nematocin mutant males (Fig. 3F and fig. S9). All defects were rescued by transgenes that spanned the nematocin gene (Fig. 3, B to E, and fig. S8).

Null mutations in the receptor genes disrupted partly overlapping aspects of the mating response. *ntr-1* was required for the initial response to hermaphrodite contact (Fig. 3D), matching *ntr-1* expression in male ray neurons that mediate this behavior (*12*). This defect was partially rescued by *ntr-1* expression in a subset of ray neurons (fig. S10). *ntr-2* had a substantial effect on overall reproductive efficiency (Fig. 3B). Both receptors were required for correct execution of turns and mating success (Fig. 3, C and E).

C. elegans males have a long-term mate search behavior in which they leave a bacterial food source that lacks hermaphrodite mating partners (*15*). Nematocin mutant males and *ntr* mutant males were partly deficient in male-typical leaving behavior, suggesting a defect in mate search (Fig. 3G). This behavioral change was not due to a general locomotion or sensory defect, because nematocin mutants had normal locomotion parameters on and off of food and normal responses to aversive stimuli, touch, and drugs (figs. S11 and S12).

The broad actions of nematocin on male mating behaviors could result from humoral secretion that activates many targets, precise release at specific neuronal sites, or a mixture of the two. To identify relevant sites of nematocin action without risking misexpression, we focused on rescue with the endogenous nematocin promoter, manipulating its precise expression pattern through Cre-mediated recombination (Fig. 4A). Cre-mediated recombination in all *ntc*-expressing cells caused defects in all male mating behaviors (fig. S13), whereas specific Cre-mediated recombination in the DVA mechanosensory neuron led to defects in initial contact response and vulva location efficiency, but did not affect turning behaviors (Fig. 4, C to F). Laser ablation of the DVA neuron caused the same defect in the hermaphrodite contact response as the DVA nematocin knockout (Fig. 4B). DVA ablation also generated striking male-specific defects in locomotion speed and posture that were not observed in nematocin mutants (fig. S14). DVA has only mild effects on hermaphrodite loco-

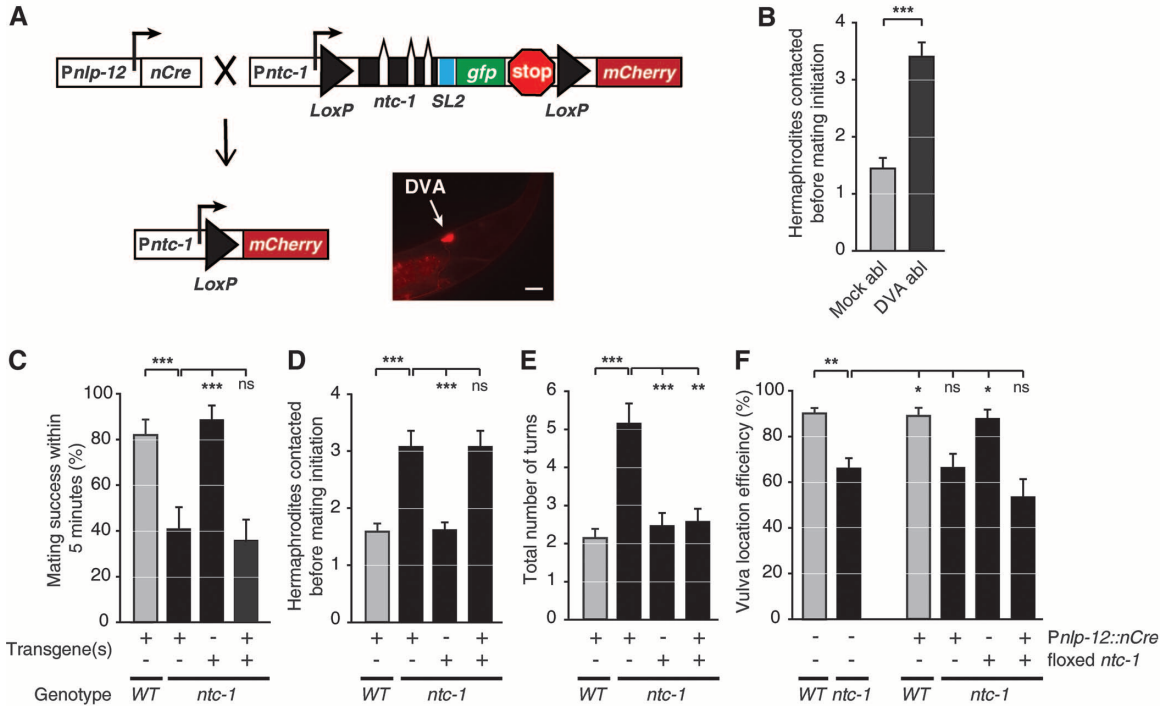

Fig. 4. Selective inactivation of *ntc-1* in DVA affects individual steps of male mating behavior. (**A**) Cre/Lox strategy to selectively inactivate *ntc-1* in DVA. (Inset) Tail of larval stage 4 male expressing mCherry and not GFP in DVA, indicating successful DVA-specific recombination. Scale bar, 10 μm. (**B** to **F**) Behavioral phenotypes of males with *ntc-1* inactivated in DVA [(C) to (F)] or after DVA laser ablation (B). (C) to (E) Behaviors as in Fig. 3. (F) Vulva location ability of males (percentage of positive vulva detections/total vulva encounters). *$P < 0.01$, **$P < 0.001$, ***$P < 0.0001$.

motion and is not obviously sexually dimorphic, so its strong male-specific effects on movement were unexpected.

These results indicate that nematocin provides a neuromodulatory input to organize diverse aspects of male mating, increasing the effectiveness by which distributed circuits generate coherent behaviors. DVA is directly proprioceptive (*10*) and also receives synaptic input from the male sensory ray neurons and mechanosensory neurons (*16*); its ability to release nematocin that activates NTR-1 on ray neurons may provide a feedback signal at the onset of mating. The DVA neuron produces additional transmitters and performs other functions, and nematocin is released from additional sources, so the functions of mating neurons and peptides are partly orthogonal (*7*, *12*, *13*). We suggest that nematocin and its receptors prime neurons in a variety of local circuits to generate a neuroethological "appetitive" function in mating. This insight refines the likely functions of oxytocin/vasopressin-related neuropeptides and suggests that they have ancient roles in reproductive behaviors that are conserved in bilaterian vertebrates, lophotrochozoa, and nematodes. The apparent conservation of oxytocin/vasopressin peptides in reproductive behavior stands in contrast with the diversity of mechanisms for sex determination, sex chromosomes, and dosage compensation (*17*).

References and Notes

1. Z. R. Donaldson, L. J. Young, *Science* **322**, 900 (2008).
2. D. A. Wagenaar, M. S. Hamilton, T. Huang, W. B. Kristan, K. A. French, *Curr. Biol.* **20**, 487 (2010).
3. J. T. Winslow, T. R. Insel, *Neuropeptides* **36**, 221 (2002).
4. M. Kosfeld, M. Heinrichs, P. J. Zak, U. Fischbacher, E. Fehr, *Nature* **435**, 673 (2005).
5. I. D. Neumann, A. H. Veenema, D. I. Beiderbeck, *Front. Behav. Neurosci.* **4**, 12 (2010).
6. Materials and methods are available as supplementary materials on *Science* Online.
7. K. Kim *et al.*, *Science* **326**, 994 (2009).
8. J. Hodgkin, *Annu. Rev. Genet.* **21**, 133 (1987).
9. I. Mori, Y. Ohshima, *Nature* **376**, 344 (1995).
10. W. Li, Z. Feng, P. W. Sternberg, X. Z. Xu, *Nature* **440**, 684 (2006).
11. C. M. Loer, C. J. Kenyon, *J. Neurosci.* **13**, 5407 (1993).
12. K. S. Liu, P. W. Sternberg, *Neuron* **14**, 79 (1995).
13. L. R. Garcia, P. Mehta, P. W. Sternberg, *Cell* **107**, 777 (2001).
14. Y. Liu *et al.*, *PLoS Genet.* **7**, e1001326 (2011).
15. J. Lipton, G. Kleemann, R. Ghosh, R. Lints, S. W. Emmons, *J. Neurosci.* **24**, 7427 (2004).
16. T. A. Jarrell *et al.*, *Science* **337**, 437 (2012).
17. H. Ellegren, *Nat. Rev. Genet.* **12**, 157 (2011).

Acknowledgments: Strains bearing *ntc-1, ntr-1,* and *ntr-2* mutations are available through the *C. elegans* National BioResource Project (NBRP), subject to a materials transfer agreement. Sequence accession numbers are as follows: NM_001038459.1 (*ntc-1*), NM_060792 (*ntr-1*), NM_078076 (*ntr-2*). We thank S. Emmons for sharing the male wiring diagram before publication; D. Anderson, S. Emmons, S. Flavell, A. Gordus, W. Kristan, T. Maniar, P. McGrath, L. Vosshall, and Y. Xu for discussions; S. Chalasani for plasmids; S. Mitani and the National Bioresource Project for *ntc-1, ntr-1,* and *ntr-2* mutants; and the Rockefeller Proteomics Facility, the Rockefeller Bioimaging Facility, and the Rockefeller High Throughput Screening Facility for technical support. This work was supported by a grant from the G. Harold and Leila Y. Mathers Foundation, by Harvey Karp and Helen Hay Whitney Fellowships to J.L.G., by NIH grant K99GM092859 to J.L.G., and by NIH grant GM07739 to E.Z.M. C.I.B. is an Investigator of the Howard Hughes Medical Institute.

Supplementary Materials

www.sciencemag.org/cgi/content/full/338/6106/540/DC1
Materials and Methods
Figs. S1 to S14
Table S1
References (*18*–*36*)

18 June 2012; accepted 9 August 2012
10.1126/science.1226201

Vasopressin/Oxytocin-Related Signaling Regulates Gustatory Associative Learning in *C. elegans*

Isabel Beets,[1] Tom Janssen,[1] Ellen Meelkop,[1]* Liesbet Temmerman,[1] Nick Suetens,[1] Suzanne Rademakers,[2] Gert Jansen,[2] Liliane Schoofs[1]†

Vasopressin- and oxytocin-related neuropeptides are key regulators of animal physiology, including water balance and reproduction. Although these neuropeptides also modulate social behavior and cognition in mammals, the mechanism for influencing behavioral plasticity and the evolutionary origin of these effects are not well understood. Here, we present a functional vasopressin- and oxytocin-like signaling system in the nematode *Caenorhabditis elegans*. Through activation of its receptor NTR-1, a vasopressin/oxytocin-related neuropeptide, designated nematocin, facilitates the experience-driven modulation of salt chemotaxis, a type of gustatory associative learning in *C. elegans*. Our study suggests that vasopressin and oxytocin neuropeptides have ancient roles in modulating sensory processing in neural circuits that underlie behavioral plasticity.

The neurohypophyseal peptides vasopressin (VP) and oxytocin (OT) are related key hormones that regulate mammalian physiology (*1*–*3*). Their gene origin dates back at least 700 million years as indicated by the presence of structurally related peptides in some invertebrate phyla (*4*, *5*). Peripheral effects of VP/OT-related peptides, primarily on water homeostasis and reproduction, are equally conserved (*5*, *6*). Mammalian VP and OT peptides can act as central nervous system mediators of social behaviors, including parental care, pair bonding, social cognition, and aggression (*7*, *8*). They also modulate vertebrate cognition in a nonsocial context, although mechanistic complexities confound a clear understanding of these effects (*9*). Here, we identify and study a VP/OT-related system in the genetically tractable model *Caenorhabditis elegans*, which displays a high level of behavioral plasticity despite its relatively simple nervous system (*10*).

Through in silico data mining of the *C. elegans* genome, we characterized 91 presumptive neuropeptide heterotrimeric guanine nucleotide–binding protein (G protein)–coupled receptor (GPCR) genes (*11*). Protein sequences of two orphan rhodopsin class GPCR genes, which we named nematocin receptors *ntr-1* (T07D10.2) and *ntr-2* (F14F4.1), clustered in the VP and OT receptor clade (fig. S1 and table S1). Sequence alignment with insect, mollusk, and mammalian VP/OT receptors revealed the presence of specific amino acid residues important for VP/OT peptide binding (fig. S2 and table S1).

To determine the cognate ligand of NTR-1 and NTR-2, we cloned and transiently expressed each receptor in Chinese hamster ovary (CHO) cells stably overexpressing apo-aequorin and the promiscuous $G\alpha_{16}$ subunit (*12*). We challenged these cells with a synthetic library of 262 known and predicted *C. elegans* peptides. NTR-1–expressing cells responded dose-dependently with a nanomolar half maximal effective concentration (EC_{50}) to a single peptide CFLNSCPYRRYamide (*13*), henceforward named nematocin (Fig. 1A). Several amino acid residues of nematocin match the neurohypophyseal peptide motif, supporting that it belongs to the VP/OT peptide family (table S2). Structural conservation is also evident at the level of its preproprotein (Fig. 1B, fig. S3, and table S3) encoded by the nematocin precursor gene *ntc-1* (F39C12.4). Similar to the architecture of VP/OT-related precursors, NTC-1 comprises a cysteine-rich neurophysin domain located immediately downstream of the mature peptide. Insect and octopus VP/OT-related peptides and a predicted, truncated form of nematocin, CFLNSCPY (*13*), were unable to activate NTR-1 (Fig. 1A and fig. S4), indicating the importance of the C-terminal nematocin residues for receptor activation. NTR-2 did not respond to nematocin or affect the dose-dependent activation of NTR-1 (fig. S5). We conclude that the VP/OT-related

[1]Department of Biology, Functional Genomics and Proteomics Unit, KU Leuven, 3000 Leuven, Belgium. [2]Department of Cell Biology, Erasmus MC, 3000 CA Rotterdam, Netherlands.

*Present address: Queensland Brain Institute, The University of Queensland, Brisbane, Australia.

†To whom correspondence should be addressed. E-mail: liliane.schoofs@bio.kuleuven.be

Supplementary Materials for

Oxytocin/Vasopressin-Related Peptides Have an Ancient Role in Reproductive Behavior

Jennifer L. Garrison, Evan Z. Macosko, Samantha Bernstein, Navin Pokala, Dirk R. Albrecht, Cornelia I. Bargmann*

*To whom correspondence should be addressed. E-mail: cori@rockefeller.edu

Published 26 October 2012, *Science* **338**, 540 (2012)
DOI: 10.1126/science.1226201

This PDF file includes:

Materials and Methods

Nematode Growth
Unless otherwise noted, strains were grown and maintained under standard conditions at 22-23 °C on nematode growth medium (NGM) 2% agar plates seeded with *E. coli* strain OP50.

Strains
Wild-type worms were Bristol variety N2. Males were maintained by setting up mating plates once per week, and fresh stocks were thawed every 3 months to avoid accumulating background mutations. Mutant strains obtained from the National Bioresource Project include *ntc-1(tm2385) X, ntr-1(tm2765) I,* and *ntr-2(tm2243) X.*

Mutant strains:
CX8634 *ntc-1(tm2385) X,* outcrossed 4X to N2
CX14102 *ntr-1(tm2765) I,* outcrossed 6X to N2
CX8633 *ntr-2(tm2243) X,* outcrossed 4X to N2
CX14101 *ntr-1(tm2765) I; ntr-2(tm2243) X*
CX4862 *dpy-5(e61) I*
CB928 *unc-31(e928) IV*
CX13503 *eat-4(ky5) III,* outcrossed 10X to N2
CX8870 *mec-3(u778) IV,* outcrossed 2X to N2
TQ296 *trp-4(sy695) I,* outcrossed 8X to N2

Mutant Alleles
ntc-1(tm2385) is a 217 bp deletion (79:295) that introduces a stop codon at amino acid residue 29. This mutation deletes part of the nematocin peptide, including post-translational processing sites, and removes the entire neurophysin domain.

ntr-1(tm2765) is a 209 bp deletion (153:361) that introduces a stop codon at amino acid residue 64 (full length NTR-1 predicted protein is 379 amino acids). This mutation truncates the protein in the first predicted transmembrane domain.

ntr-2(tm2243) is a 3 bp insertion (GTA at bp 2,441) followed by a 1,140 bp deletion (2,441:3,580) that introduces a stop codon at amino acid residue 66 (full length NTR-2 predicted protein is 398 amino acids). This mutation truncates the protein in the second predicted transmembrane domain.

Molecular biology and generation of transgenic lines
The genomic region of *ntc-1* was amplified using 5′-atgggctcctcacctatcctc-3′ and 5′-ttaacacattgcacttgtttgacatc-3′ primers.

The *ntr-1* cDNA was amplified with 5′- atgggagccttctttcctgtc -3′ and 5′- tcaaaaatcgctttgctcactg -3′ primers, from RNA that was isolated from N2 animals and reverse-transcribed into cDNA. The cDNA isolated matched the prediction from www.wormbase.org (WS231).
The *ntr-2* cDNA was amplified with 5′-atgaacaacaacacgttgaacataac-3′ and 5′-ttaattagagttggtcttcaaggaagtag-3′ primers, from RNA that was isolated from N2 animals and

reverse-transcribed into cDNA. The cDNA isolated matched the prediction from www.wormbase.org (WS231).

All promoters were amplified from N2 wild-type mixed stage worm genomic lysates. The sequences of the primers used are shown below:

Pntc-1: 5'-tcatgtttgcataaactccaaaatt-3', 5-gttggaatggaaagtgaagattg-3'
Pntr-1: 5'-gttgccacagtgaggactcgaa-3', 5'-gctcccatgattgaacacg-3'
Pntr-2: 5'-atcagagattgtctcctct-3', 5'-cgtgttgttgttcatgctgaaatc-3'
Pnlp-12: 5'-cctacccatcaacctagtttccg-3', 5'-tttgtcggaggcaattgaaat-3'
Ptph-1: 5'-gtcttcccgcttgcaatactaatag-3', 5'-atgattgaagagagcaatgctaccta-3'
Pgcy-8: 5'-tggtctgcttctggactg-3', 5'-gaatatgagttgataaaaatgtacgaaatg-3'
Psrh-220: 5'-gattctcaaagagcaatgttcc-3', 5'-acttgagtttggaccgaaaagc-3'
Pflp-6: 5'- tcccgtacctttttccttcct-3', 5'-attctggaataatcatattgttttcaa-3'

The *ntc-1* genomic region and *ntr-1* and *ntr-2* cDNAs were inserted into pSM vectors using NheI and KpnI restriction enzymes. Promoter regions were cloned into pSM vectors using FseI and AscI restriction enzymes.

For mammalian expression, the *ntr-1* and *ntr-2* cDNAs were amplified from pSM vectors with 5′-gccgccatgggagccttctttcctgtca-3′, 5′-gtcaaaaatcgctttgctcactg-3′ (*ntr-1*), and 5′-gccgccatgaacaacaacacgttgaacataacc -3′, 5′-gttaattagagttggtcttcaaggaagtagag-3′ (*ntr-2*) primers using Easy-A high fidelity polymerase (Agilent) to generate PCR products with 5' Kozak concensus sequence and 3'-A overhangs. These were inserted separately into the PCDNA3.3 TOPO TA cloning vector (Invitrogen) according to the manufacturer's instructions.

For selective expression of transgenes using Cre-Lox, one *LoxP* site was inserted between the promoter (AscI) and gene (NheI) cloning sites of the *pSM Pntc-1*::*ntc-1 SL2::GFP* vector and a second *LoxP* site followed by the mCherry sequence was inserted downstream of the GFP stop codon. *ntc-1* and *nlp-12* promoters were cloned into *pSM-Cre* (*18*) using the FseI and AscI sites.

Extrachromosomal transgenes
Transgenes were made by injection of DNA clones into the gonads of young adult hermaphrodites together with a fluorescent coinjection marker using standard protocols (*19*). To control for variation between transgenes, two to three independent lines from each injection were characterized for all behavioral assays and expression patterns.

Transgenic strains

CX11850, CX11851 *kyEx3223, kyEx3224 [Pntc-1::GFP @ 100ng/μL]*
CX14186, *kyEx4438 [Pntc-1::mCherry @ 30 ng/μL]*
CX7847 *kyEx1141 [Pntr-1::GFP @ 30 ng/μL]*
CX7848, CX7849, *kyEx1142, kyEx1143 [Pntr-2::GFP @ 100 ng/μL]*
CX7844, CX7845, *ntr-1(tm2765) I, kyEx1138 CX7845 [Pntr-1::ntr-1::SL2::GFP @ 100 ng/μL]*
CX14197, CX14198, *ntc-1(tm2385) X; kyEx4449, kyEx4450 [Pntc-1::ntc-1::SL2::GFP @ 20 ng/μL]*

CX14187, CX14200, CX14199, *ntc-1(tm2385) X; kyEx4439, kyEx4452, kyEx4451 [Pntc-1::nCre @ 1 ng/μL; Pofm-1::dsRed2 @ 15 ng/μL]*

CX14201 *ntc-1(tm2385) X; kyEx4453 [Pnlp-12::nCre @ 1 ng/μL; Pofm-1::dsRed2 @ 15 ng/μL]*

CX14194-CX14196, *ntc-1(tm2385) X; kyEx4446-kyEx4448 [Pntc-1::Lox::ntc-1::SL2::GFP::LoxP::mCherry @ 20 ng/μL]*

CX15170-CX15172, *ntr-1(tm2765) I ; kyEx5079-kyEx5081 [Pflp-6::ntr-1::SL2::GFP @ 20 ng/μL; Pmyo-2::mCherry @ 2 ng/μL]*

CX15174, *kyEx5083 Ex[ntr-2^{FOSMID}(WRM062aE11)::NLS::GFP @ 10 ng/μL; Pmyo-2::mCherry @ 2 ng/μL]*

CX15175, *kyEx5084 Ex[ntr-1^{FOSMID}(WRM062aE11)::NLS::GFP @ 50 ng/μL; Pmyo-2::mCherry @ 2 ng/μL]*

CX15177, *kyEx5086 Ex[ntr-1^{FOSMID}(WRM066D10)::NLS::GFP @ 10 ng/μL; Pmyo-2::mCherry @ 2 ng/μL]*

CX15179, *kyEx5088 Ex[ntc-1^{FOSMID}(WRM0638cG07)::NLS::GFP @ 10 ng/μL; Pmyo-2::mCherry @ 2 ng/μL]*

CX15180, *kyEx5089 Ex[ntr-1^{FOSMID}(WRM066D10)::NLS::GFP @ 50 ng/μL; Pmyo-2::mCherry @ 2 ng/μL]*

CX15181, *kyEx5090 Ex[ntc-1^{FOSMID}(WRM0638cG07)::NLS::GFP @ 50 ng/μL; Pmyo-2::mCherry @ 2 ng/μL]*

CZ1758, *juIs76 [Punc-25::GFP]*

EG1285, *lin-15(n765) X, oxIs12 [Punc-47::GFP]*

VM133, *lin-15(n765) X, akEx31 [Pglr-5::GFP]*

PS3228, *pha-1(e2123ts) III; him-5(e1490) X, syEx313 [Ppkd-2::GFP]*

RW10222, *zuIs178[Phis-72(1kb)::HIS-72::GFP]; stIs10029[Ppie-1::H2B::GFP]*

CX15256, *ntc-1(tm2385) X, zuIs178[Phis-72(1kb)::HIS-72::GFP]; stIs10029[Ppie-1::H2B::GFP]*

NTC-1 peptide synthesis

Materials obtained from commercial sources were reagent grade and used without further purification. HPLC grade solvents, trifluoroacetic acid, and 4,4′-Dithiodipyridine (4-PDS, Aldrithiol™-4, CAS Number 2645-22-9) were obtained from Sigma-Aldrich. Crude linear NTC-1 peptide (CFLNSCPYRRY-amide) was synthesized by the Rockefeller University Proteomics Facility with a Symphony Peptide Synthesizer (Protein Technologies) using standard FMOC-based chemistry. The Fmoc amino acid intermediates were from Anaspec, Inc. The crude peptide was purified by preparative reverse phase high performance liquid chromatography (HPLC) on a Peeke Scientific Duragel-G 5 μm preparative C18 column (50 × 20 mm, flow rate 5 ml/min) using a Varian ProStar 210 solvent delivery system equipped with a ProStar 325 dual wavelength UV/Vis detector (monitoring at 215 and 245 nm) and a ProStar 701 fraction collector (5 ml fractions) using a linear aqueous gradient of acetonitrile (CH_3CN) and 0.1% trifluoroacetic acid (TFA). The NTC-1 peptide eluted in ~58% CH_3CN/0.1% TFA. Fractions containing NTC-1 peptide were pooled and divided into two samples: one sample (NTC-1 linear reduced peptide) was lyophilized and used for experimental controls; the other was cyclized (see below) to yield the mature NTC-1 synthetic peptide.

NTC-1 peptide cyclization

Intramolecular disulfide bond formation was carried out using 4,4′-Dithiodipyridine (4-PDS) essentially as described (*20*). Briefly, HPLC fractions containing purified NTC-1 linear peptide in ~58% CH_3CN/0.1% TFA (pH ~1.8) were pooled and approximate peptide concentration was determined by measuring absorption at 280 nm with an Ultrospec 2100 Pro UV/Vis spectrophotometer (GE Healthcare) and dividing by the peptide absorbance coefficient determined by ProtParam (www.exasy.org). If necessary, the peptide concentration was adjusted to between 10 – 100 μM with aqueous 50% CH_3CN/0.1% TFA. 4-PDS (freshly prepared 10 mM CH_3OH stock, 1.2 eq) was added dropwise directly to the peptide while stirring. The reaction was stirred at room temperature for 1-3 h and reaction progress monitored by HPLC on a Peeke Scientific Duragel-G 5 μm analytical C18 column (250 × 46 mm, flow rate 1 ml/min) using a linear aqueous gradient of 1 – 90% CH_3CN/0.1% TFA and monitoring at 215 nm (peptide) and 320 nm (reagent). When oxidation was complete, the crude reaction mixture was concentrated to 1/10 the original volume to remove the CH_3CN on a rotary evaporator. The concentrated crude reaction mixture was applied directly to a C18-SepPak column (Waters, pre-equilibrated with 10 ml ddH_2O/0.1 % TFA) using a peristaltic pump (Rainin Dynamax RP-1, speed = 5.00). The column was washed first with 10 ml ddH_2O/0.1% TFA (Wash 1) to remove the thiopyridine by-product, then with 10 ml aqueous 2% CH_3CN/0.1% TFA (Wash 2) to remove the unreacted 4-PDS reagent. The oxidized NTC-1 peptide was eluted with 10 ml aqueous 50% CH_3CN/0.1% TFA and lyophilized. Both the linear reduced and cyclized NTC-1 peptides were verified by LC-ESI-MS using a Waters 2695 Separations Module (Xterra MS C18 column (Waters), flow rate 0.2 ml/min) connected inline to a Waters ZQ mass detector.

Cell culture and transfection

Human embryonic kidney 293T cells (HEK293T) were cultured in DMEM supplemented with 10% FBS at 37 °C in a humidified atmosphere containing 5% CO_2. Cells were plated in either 35 mm MatTek glass bottom dishes (for calcium imaging) or 10 cm dishes (for cAMP HTRF assays) and when they reached 60 – 70% confluency were transfected with a 1:1 ratio of PCDNA3.3 containing ~ 1 μg *ntr-1* or *ntr-2* cDNA and pcDNA3-α15Z (encoding promiscuous G protein 15, a gift from Y.H. Wang) using Lipofectamine 2000 and incubated for 24 h at 37 °C, then transferred to 28 °C and incubated for another 16-24 h (*21*). For control experiments, empty vector, the receptor or G protein was transfected alone. Experiments were conducted on three plates for each condition on three different days.

Calcium imaging

Calcium imaging experiments were conducted essentially as described (*22*). The transfected cells were loaded with 2.5 mM fura-2/AM (Invitrogen) for 25 min at 37 °C. Synthetic peptides diluted in Ringer's solution were applied sequentially to the cells for 15 s with a peristaltic pump, and fluorescence at 510 nm was monitored (excitation at 340/380 nm) using a MetaFluor calcium imaging system with a Nikon Eclipse TE2000U microscope. The calcium response was calculated using cells in randomly chosen fields. In all figures, averages and s.e.m. are shown from at least 100 single cell responses from three independent experiments. The half-maximal effective concentrations for NTC-1 cyclized peptide to activate cells transfected with NTR-1 and Gα15 (EC_{50} value) was calculated using Prism (GraphPad Software) using nonlinear regression.

cAMP detection

cAMP concentration in transfected HEK293T cells was measured with a homogeneous time resolved fluorescence resonance energy transfer (HTR-FRET) method using the HTRF cAMP Dynamic kit (CisBio International) according to the manufacturer's instructions. Assays were performed in 96-half well plates using 4,000 cells/well and 384-well plates using 2,000 cells/well. In brief, cells were pre-incubated for 40 min with 1 mM IBMX diluted in serum-free DMEM media, then stimulated for 15 min at 37 °C with 5 μM forskolin in the presence or the absence of NTC-1 peptide (*7*). The cells were lysed in lysis buffer containing the FRET acceptor cAMP-d2 and anti-cAMP Cryptate was added. After 60 to 90 min incubation at room temperature, the TR-FRET signal was measured using a Wallac 2100 Envision Microtiter Plate Reader (Perkin Elmer) in the Rockefeller University High Throughput Screening Facility. The signal was quantified with Wallac Envision Manager. Assays were performed in duplicate with three independent biological samples and the results were analyzed by nonlinear regression (GraphPad).

Neuropeptide isolation

Total neuropeptides were isolated from wild-type N2 worms using published procedures *(23*) with minor modifications. Mixed stage worms (males and hermaphrodites) were grown on large NGM plates seeded with OP50 bacteria at 15 °C, rinsed from plates with cold S-basal buffer, and excess bacteria removed by 30% sucrose flotation. The resulting worm pellet was washed with ddH_2O containing a freshly dissolved protease inhibitor cocktail tablet (mini EDTA-free, Roche). The worms were centrifuged at 500 *g* for 2 min, the supernatant was removed, then the pellet was flash frozen in liquid N_2 and stored at -80 °C. Worm pellets from multiple isolations were thawed on ice and combined in a dounce homogenizer. Cold extraction buffer was added (methanol:water:acetic acid, 90:9:1 vvv) and worms were homogenized with 10 strokes on ice, then sonicated for 2 min, then chilled on ice for 2 min. The dounce/sonicate/chill cycle was repeated three times. The mixture was transferred to a 50 ml conical tube and centrifuged for 15 min at 3,000 rpm at 4 °C. The pellet was discarded and the methanol removed from the supernatant by rotary evaporation. The residual aqueous fraction was re-extracted with ethyl acetate and hexanes to remove lipids. The aqueous phase was desalted using a SepPak C18 column (Waters, pre-equilibrated with ddH_2O/0.1 % TFA) using a peristaltic pump (Rainin Dynamax RP-1, speed = 5.00). The column was washed with ddH_2O/0.1% TFA and peptides were eluted in 50% CH_3CN/0.1% TFA; particles were removed by centrifugation through a 0.22 μm spin filter (VWR). Filtered neuropeptides were fractionated by HPLC on a Peeke Scientific Duragel-G 5 μm analytical C18 column (250 × 46 mm, flow rate 1 ml/min). The column was washed for 10 minutes with 2% CH_3CN/0.1% TFA, then peptides were eluted in a 4-step linear gradient over 70 minutes: 0 – 20 min, 2 – 22% CH_3CN/0.1% TFA; 20 – 50 min, 22 – 37% CH_3CN/0.1% TFA; 50 – 60 min, 37 – 50% CH_3CN/0.1% TFA; and 60 – 70 min, 50 – 100% CH_3CN/0.1% TFA. Synthetic cyclized NTC-1 peptide was run in parallel using the same column and solvent gradient for comparison and 5 fractions surrounding the retention time corresponding to the NTC-1 peptide were selected for analysis by mass spectrometry.

Mass spectrometry

Tandem mass spectrometry (MS/MS) was performed on an LTQ Orbitrap XL hybrid FTMS (Fourier Transform Mass Spectrometer, Thermo Scientific) in the Rockefeller University Proteomics Facility. HPLC fractions from total N2 neuropeptide isolations were lyophilized and resuspended in 20 μl of water. LC (liquid chromatography) was performed with the Ultimate

3000 HPLC system (Dionex). Samples were injected onto a custom-made C18 analytical column (75 μm diameter beads and C18 5 μm trap column from LC Packings) with a 60 min gradient of CH_3CN/0.1% formic acid. The flow rate through the trap column was 30 μl/min and the flow rate through the analytical column was 0.2 μl/min. Online MS/MS analysis was performed on the LTQ Orbitrap XL ion trap in positive ion mode with a mass range of 400 - 1600 m/z (mass to charge ratio). MS fragmentation analysis was performed on the ion of the highest intensity observed at 30 ms intervals.

Microscopy

For all microscopy, live animals were mounted on 2% or 4% agarose pads containing 400 mM tetramisole or 5 mM sodium azide. Images were collected with a 40×, 63×, or 100× objective on a Zeiss Axioplan2 imaging system with a Hamamatsu Photonics C2400 CCD camera, a Zeiss Axio Imager.Z1 with ApoTome with a Zeiss AxioCam MRm CCD camera, or a Zeiss Axio Observer Z1 LSM 780 laser scanning confocal microscope. Wide-field fluorescence images were obtained on a Zeiss Axioplan2 imaging system. Images were processed in Metamorph, Image J and Adobe Photoshop.

Expression patterns

Cells expressing GFP were identified by Nomarski microscopy in both larval and adult hermaphrodites and males. In addition to identifying cells based on their position within the animal and distinctive processes, the identification of some cells was aided by crossing *ntc-1* or *ntr-1* promoter-GFP or promoter-mCherry expressing animals with promoter-mCherry or promoter-GFP fusions with established expression patterns. In this manner, the DVA neuron was identified based on its position and co-localization with *Pnlp-12::mCherry*; AFD neurons were identified based on co-localization with *Pgcy-8::GFP*; ADL neurons were identified based on co-localization with *Psrh-220::GFP*; AVK neurons were identified based on co-localization with *Pglr-5::GFP*; NSM neurons were identified based on co-localization with *Ptph-1::GFP*; the HOB neuron was identified based on co-localization with *Ppkd-2::GFP*; and GABAergic ventral cord motor neurons were identified based on partial co-localization with *Punc25::GFP* and *Punc-47::GFP*. Fosmid recombineering was carried out as described using the pBALU9 vector (NLS GFP)(*24*). For each GFP fusion gene, multiple transgenic lines were examined.

Immunofluorescence

Rabbit polyclonal antisera (YZ2579 and YZ2580) against synthetic nematocin peptide were generated using genomic antibody technology by YenZym Antibodies, LLC, and used at 1:200 dilution for immunostaining. Antisera were affinity purified against cyclized synthetic nematocin peptide and tested for cross-reactivity to linear synthetic nematocin peptide. Two separate purified antibody fractions were used for immunostaining, one that specifically recognizes the mature (cyclized) nematocin peptide, and one that cross reacts with both the cyclized and linear (reduced) nematocin peptides. Affinity purified fractions from two rabbits yielded similar nematocin staining results. G10362 α-GFP (rabbit monoclonal, Invitrogen) was used at 1:200. The secondary antibodies, Alexa Fluor 488–conjugated goat α–mouse IgG, Alexa Fluor 488–conjugated goat α–rabbit IgG and Alexa Fluor 594–conjugated goat α–rabbit IgG (Invitrogen) were used at 1:400 or 1:4000 dilutions. Whole mount immunostaining was performed according to the peroxide tube fixation protocol, except that worms were fixed in 2% paraformaldehyde as described previously (*25*). Briefly, nematodes were rocked in the fixation

solution for 20 min at 21–23 °C before freezing, and overnight at 4 °C after freezing. Fixed worms were permeabilized in TTB buffer (100 mM Tris pH 7.4, 1% Triton X-100, 1 mM EDTA buffer) containing 1% β-mercaptoethanol for 2 h rocking at 37 °C, washed with BO_3 buffer (10 mM H_3BO_3 pH 9.4, 0.1% Triton X-100), reduced by 15 min incubation with 10 mM dithiothreitol in BO_3 buffer at 37 °C, then washed with BO_3 buffer. Sulfhydryl groups were oxidized by gentle agitation with BO_3 buffer containing 1% H_2O_2 for 1 h at 25 °C. Samples were washed and incubated for 15–30 min with ABB buffer (PBS containing 0.5% Triton X-100, 1 mM EDTA, 0.05% sodium azide and 0.1% BSA) and stored at 4 °C in ABA buffer (PBS containing 0.5% Triton X-100, 1 mM EDTA, 0.05% sodium azide and 1% BSA) until further use. Worms were gently rocked and incubated overnight at 4 °C in primary antibody solutions in ABA buffer, washed with ABB buffer, then rocked in secondary antibody solutions in ABA buffer for 2 h at 21–23 °C and washed with ABB buffer. Stained worms were mounted on 2% agarose pads containing 50 mM Tris pH 8.5, and 5 mM $MgCl_2$ for visualization. For dual labeling of nematocin and soluble GFP, the protocol was modified as follows: worms were pre-chilled on ice 10 min before addition of fixative and were incubated in fixative for 15 min at 21–23 °C, followed by a flash freeze-thaw cycle, followed by incubation overnight at 4 °C. Primary antibody and secondary antibody incubations were both carried out overnight at 4 °C, followed by washes in ABB buffer at 21–23 °C. Alexa Fluor 594 goat α–mouse IgG was used with α-nematocin, and Alexa Fluor 488 goat α–rabbit IgG was used with α-GFP.

Reproductive efficiency

L4 males were separated from hermaphrodites and placed on standard OP50-seeded NGM plates to develop overnight at 15 °C to ensure that the males scored were virgins. Mating efficiency was scored as described (*26, 27*) with the following modifications. One virgin male was placed with one *dpy-5* L4 hermaphrodite on an unseeded NGM plate and incubated at 20 °C. The OP50 on the worm pick used to transfer animals provided a sufficient amount of food for the worms. Efficiency was scored by counting the numbers of *dpy* and non-*dpy* progeny. Each plate was considered a single mating trial, and 10 plates per genotype were scored. Mating efficiencies were calculated as the percentage of cross progeny divided by the number of total progeny. All assays were conducted blind to genotype.

Mating behavior

Established behavioral tests were used to compare mating of wild-type and mutant males (*12*). Because mating assays are very sensitive to ambient conditions, care was taken to use exactly the same procedures for every assay conducted; even so, only assays carried out in common blocks are analyzed together in each Figure panel. NGM plates used for assays were less than 1 week old and allowed to dry upright, covered, on the bench top for 24 h before seeding. Mating lawns were seeded with 5 μl of an OP50 culture (OD_{600nm} = 1.0) and left to dry on the bench overnight. Hermaphrodites and males used for mating assays were maintained on OP50 plates at a low population density and never allowed to starve. The day before a mating assay, L4 males were separated from hermaphrodites and placed on standard OP50-seeded NGM plates to develop overnight at 15 °C to ensure that the males scored were virgins (at a density of no more than 30 males per plate). All assays were conducted blind to genotype. Young adult *unc-31* hermaphrodites were used as mating partners because they move infrequently on food and therefore allow facile observation of mating events. Virgin males were moved to room temperature for at least 2 h before beginning mating assays. For each assay, 25 – 30 young adult

unc-31 hermaphrodites (24 – 48 post L4 larval stage) were placed on a mating lawn and allowed to settle for at least 1 h before beginning the assay. A single male was transferred to the edge of the lawn and behavior was scored by direct observation at a Wild Heerbrugg M5Z dissecting microscope. Timing began when the male's tail first came in to contact with a hermaphrodite, and observation continued for 5 min or until sperm was transferred. The total number of hermaphrodites that each male contacted with his tail was scored, as well as the number and quality of turns made around the hermaphrodite's body during mating. Turn quality was analyzed as described (*11*). The ability of wild-type and mutant males to locate the vulva was measured as described (*13, 28, 29*), and scored as successful when the male paused for more than 1 s with its copulatory bursa opposed to the hermaphrodite's vulva. Vulva location efficiency was calculated as the number of successful vulva detections divided by the total number of vulva encounters. Sperm transfer was considered mating success. A minimum of 25 males were tested per genotype on at least 3 separate days. For DVA ablated males, the number of hermaphrodites that each operated male contacted with his tail before initiating mating was scored without timing; 20 males were tested on 3 separate days.

Mate searching behavior

Leaving assays were conducted as described previously (*15*). Briefly, large diameter NGM plates were seeded with 10 μl of OP50 (OD_{600nm} = 1.0) and allowed to dry on the bench overnight, resulting in a ~ 1 cm diameter lawn. Assay reproducibility depended greatly on the age and dryness of the NGM plates and on the ambient level of humidity in the lab. NGM plates used in this assay were less than 1 week old and allowed to dry upright (covered) at room temperature for 2 days before seeding. To test whether or not the plates had reached the appropriate level of dryness, a worm pick was dragged across the surface of the agar without puncturing the agar. Plates with the correct moisture content showed transient appearance of liquid trailing behind the pick that was quickly absorbed back into the agar and did not show any permanent grooves in the agar after the pick was removed. The day before an assay, L4 males were separated from hermaphrodites and placed on standard OP50-seeded NGM plates to develop overnight at 15 °C, thus ensuring that the males scored were virgins (at a density of no more than 30 males per plate). All assays were conducted blind to genotype. A single male was transferred to the center of the lawn and leaving behavior was scored by direct observation at a Wild Heerbrugg M5Z dissecting microscope with the power supply set to 3 V AC once per hour for 8 hours, then again after 24 hours. In a typical assay, 10 – 20 males of each genotype were placed individually on assay plates. Leaving was scored as positive when the male traveled more than 3 cm from the edge of the lawn. Assays were conducted on at least three separate days. Data are presented as the fraction of animals that have not left the bacterial lawn.

Brood size

Individual L4 hermaphrodites were transferred onto normal OP50-seeded NGM growth plates. Each day thereafter, the mothers were transferred to new seeded plates daily until the mother either stopped producing offspring or died. Care was taken when transferring the mother to avoid mechanical damage from the worm pick. The progeny of the previous plate were counted the next day. The total number of progeny from all plates were added to give the final brood size for each mother. Worms that crawled off the plates, bagged, or ruptured were removed from the data set. Eight to ten hermaphrodites were assayed for each genotype. All assays were conducted blind to genotype.

Locomotion parameters

For assays off food, ~20 young adult animals were picked off of their growth plates to a plate without bacteria where they were allowed to crawl away from any residual bacteria that was transferred with the worm. Animals were then transferred to the center of an assay plate with $CuCl_2$ barrier and recording begun within 2 minutes of removal from food. For assays on food, thin bacterial lawns of *E. coli* OP50 were made by seeding the entire surface of NGM plates for overnight growth at 37°C and returning them to room temperature for at least 1 h before the assay. ~20 young adult animals were picked to the assay plates and allowed to adjust to the thin lawn for at 30 min before movies were recorded. Recordings were made at 3 fps for 15 min on a digital camera (Pixelink PL-A741, set to binning 2) connected to a Carl Zeiss Stemi 2000-C stereomicroscope equipped with a 0.3x objective, and the 28 mm x 28 mm arena was captured in a 512 x 512 pixel area. Each experiment was carried out 3-9 times (~20 animals/experiment) for data shown in Supplementary Figs. S7 and S11. Movies were analyzed by Matlab-based tracking software adapted from the Parallel Worm Tracker as described (*30, 31*).

Laser ablation

Laser ablations were conducted with a Micropoint nitrogen-pumped dye laser as described (*32*). DVA neurons were killed at late L1/early L2 stage. Operated animals were kept in groups of 5–10 on OP50 NGM plates at 20 °C, and their behaviors were observed 18–24 h after L4 lethargus, in young adult animals.

Statistical tests

GraphPad Prism 5 software was used to perform statistics on all data.

Figure 1F, ANOVA with Tukey's test for multiple comparisons.

Figure 3B-3E, ANOVA with Dunnett test.

Figure 3G, One-way repeated measures ANOVA with Tukey's test for multiple comparisons.

Figure 4, ANOVA with Dunnett or Mann-Whitney test.

Supplementary Fig. S1

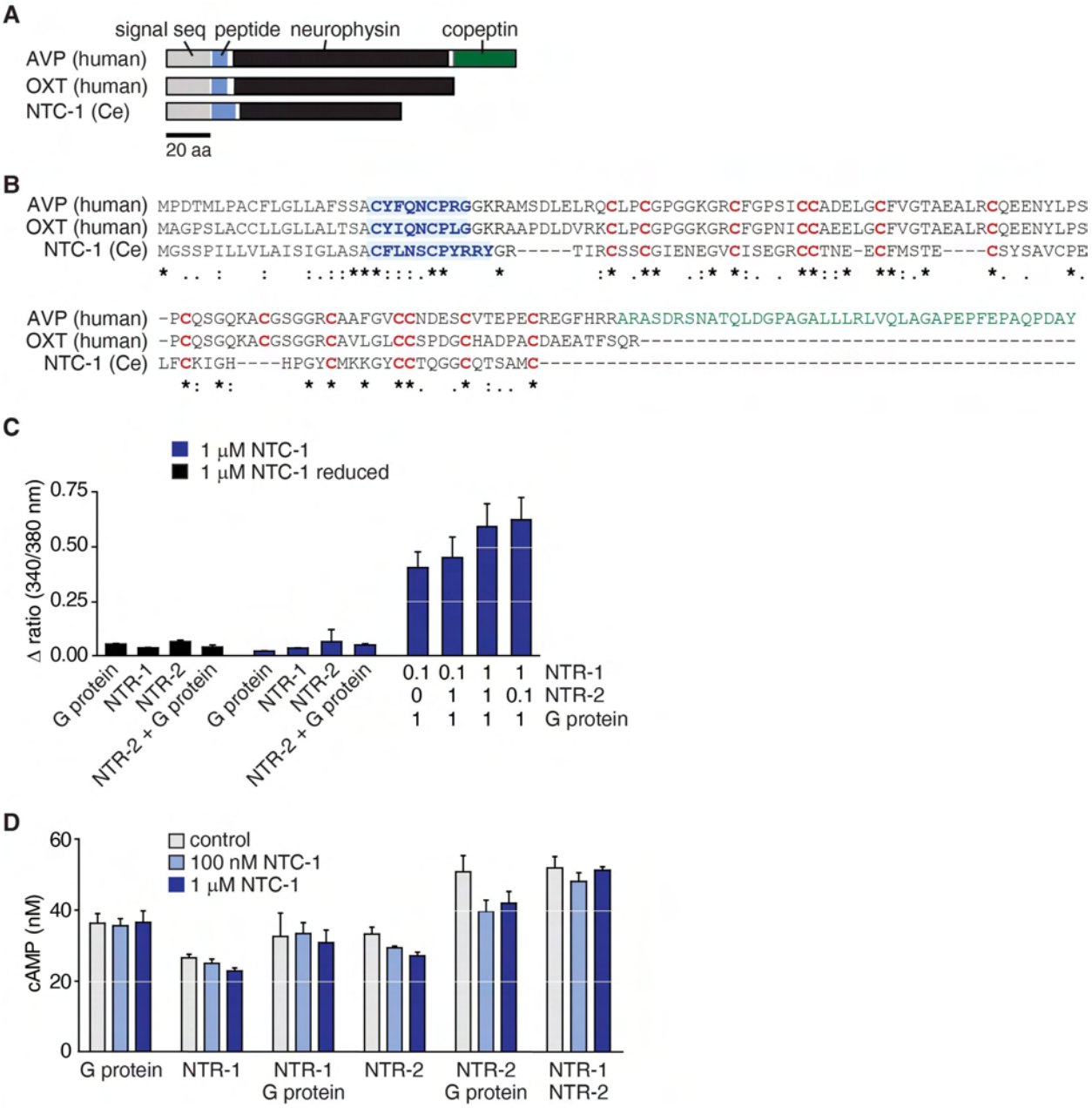

Fig. S1. (**A** and **B**) Domain structure and sequence of nematocin (*ntc-1)*, F39C12.4. The predicted open reading frame of the propeptide begins with a signal sequence, followed by a short amino acid sequence that resembles vasopressin and oxytocin, and ends with a ~100 amino acid long region with substantial similarity to the cysteine-rich neurophysin domain that facilitates oxytocin and vasopressin folding and packaging into dense core secretory vesicles (*33*). Vasopressin and oxytocin are nine residue peptides with an intramolecular disulfide bridge between cysteines 1 and 6, and charge conservation at residues 3 (hydrophobic) and 4 (polar). The *C. elegans* homolog has cysteines at positions 1 and 6, a leucine (hydrophobic) at position 3,

and an asparagine (polar) at position 4, preserving features of this architecture. Neuropeptide precursors in *C. elegans* and in mammals are cleaved at basic sites by endopeptidases, and if the peptide ends in a C-terminal glycine it is converted to an amide. The *C. elegans* vasopressin/oxytocin related peptide precursor contains three possible endopeptidase cleavage sites, one of which would encode a peptide with a C-terminal glycine. (**C**) Mean calcium responses of fura-2/AM loaded HEK293T cells transfected with indicated combinations of *ntr-1*, *ntr-2*, and Gα15 and exposed to synthetic NTC-1 peptide. Linearized (reduced) synthetic NTC-1 was used as a control. Numbers refer to the relative molar quantities of DNA used for transfection. (**D**) Forskolin-stimulated cAMP production in NTC-1-treated HEK293T cells transfected with indicated combinations of *ntr-1*, *ntr-2*, and Gα15. Error bars in all figures indicate s.e.m.

Supplementary Fig. S2

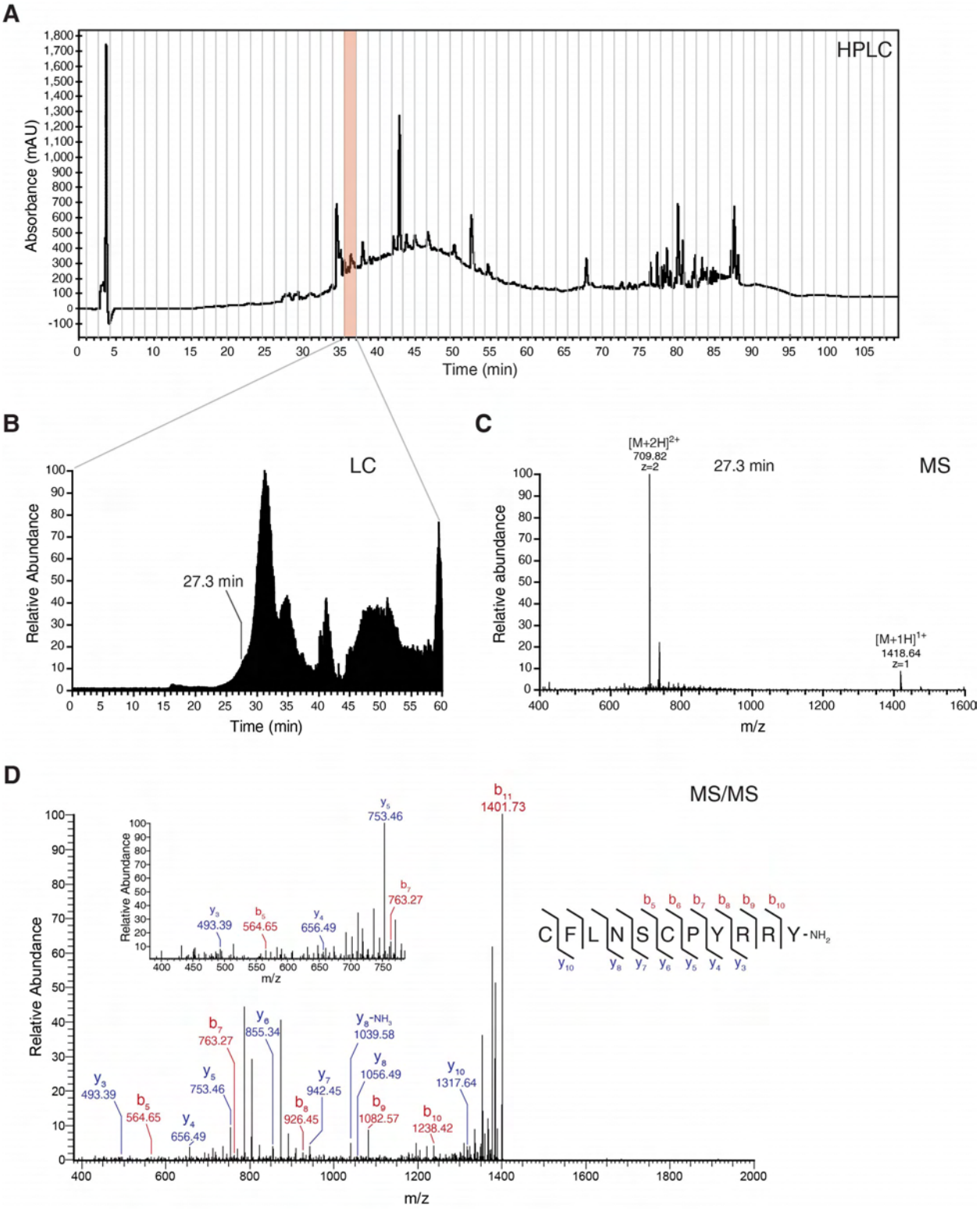

Fig. S2. Isolation and characterization of the mature NTC-1 peptide from wild-type worms. (**A**) High pressure liquid chromatography (HPLC) chromatogram of total neuropeptides isolated from N2 (wild-type) *C. elegans*. Fraction # 25 (orange bar) was selected for characterization by mass spectrometry. Absorbance was measured at 215 nm; mAU, arbitrary units. (**B**) Nano LC spectrum of TIC (total ion count) of HPLC fraction 25 over time. (**C**) Nano LC mass spectrum (MS) of the peak at 27.3 min. Ion peaks corresponding to the singly ($[M+H]^{1+}$) and doubly ($[M+2H]^{2+}$) charged NTC-1 peptide are indicated. m/z, mass to charge ratio. (**D**) Nano LC-MS/MS spectrum of the m/z 1418.64 precursor ion corresponding to the singly charged mature NTC-1 peptide. Electron transfer dissociation fragmentation confirms the sequence CFLNSCPYRRY-amide; b-type and y-type ions are indicated in the spectrum. Mass accuracy was measured with 2.96 ppm error.

Supplementary Fig. S3

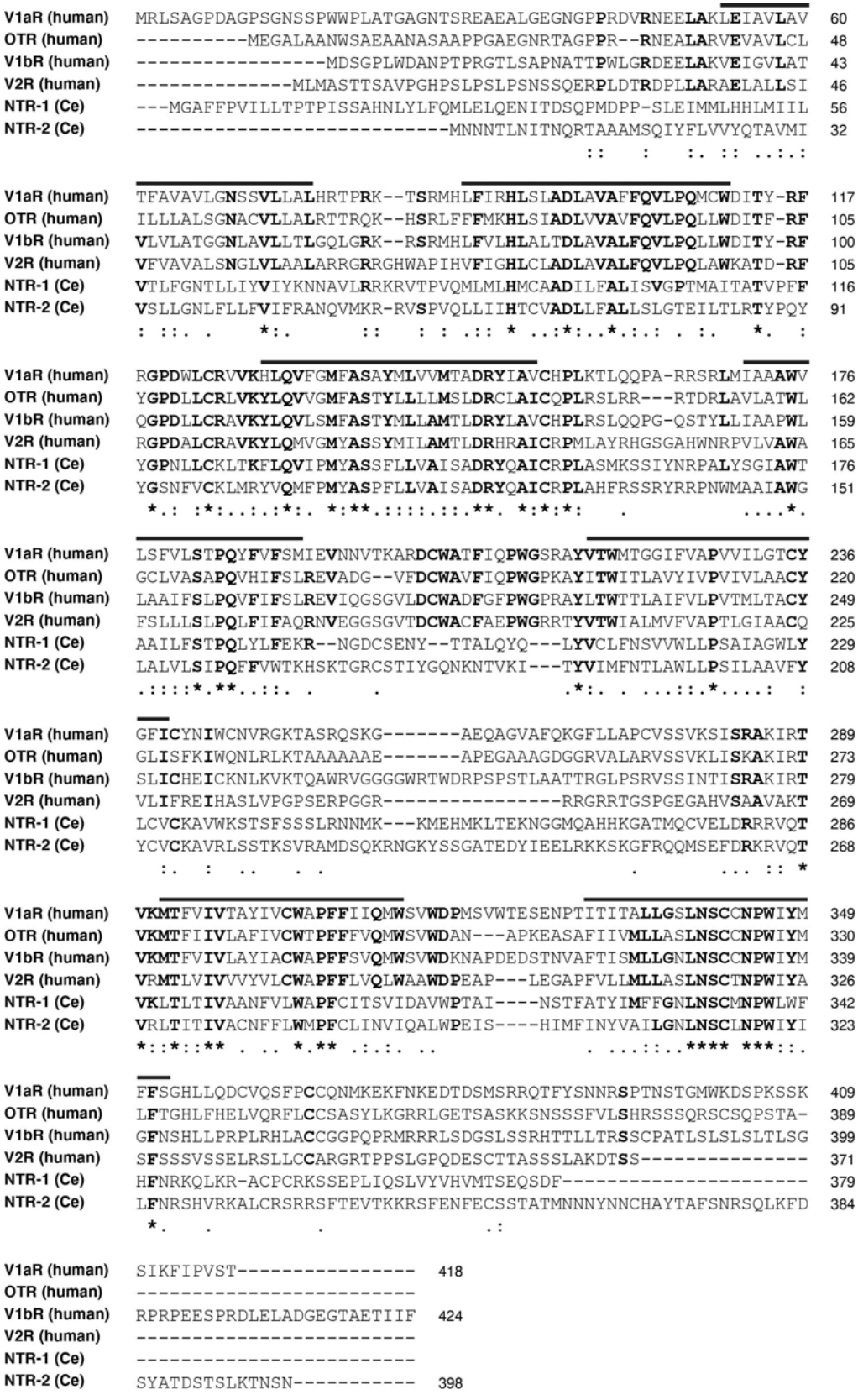

Fig. S3. Sequence alignment of *C. elegans* NTR-1 (T07D10.2) and NTR-2 (F14F4.1) with human vasopressin and oxytocin receptors. Mammalian vasopressin and oxytocin signal through four related G protein-coupled receptors (GPCRs), the V1a, V1b, and V2 vasopressin receptors and the oxytocin receptor (OT). The predicted NTRs share approximately 30% amino acid identity and 50% similarity with mammalian receptors. Amino acids that are identical between four or more sequences are in boldface type. The transmembrane domains for Vasopressin 1a receptor (V1aR) are indicated by black bars above the sequence. Asterisks (*) denote identical residues; dots (•) mark similar residues. The alignment was performed with Clustal W. Accession numbers of sequences used in the alignment: NP_000697.1 (V1aR), NP_000698.1 (V1bR), NP_000045.1 (V2R), NP_000907.2 (OTR), NP_493193.1 (NTR-1), NP_510477.1 (NTR-2).

Supplementary Fig. S4

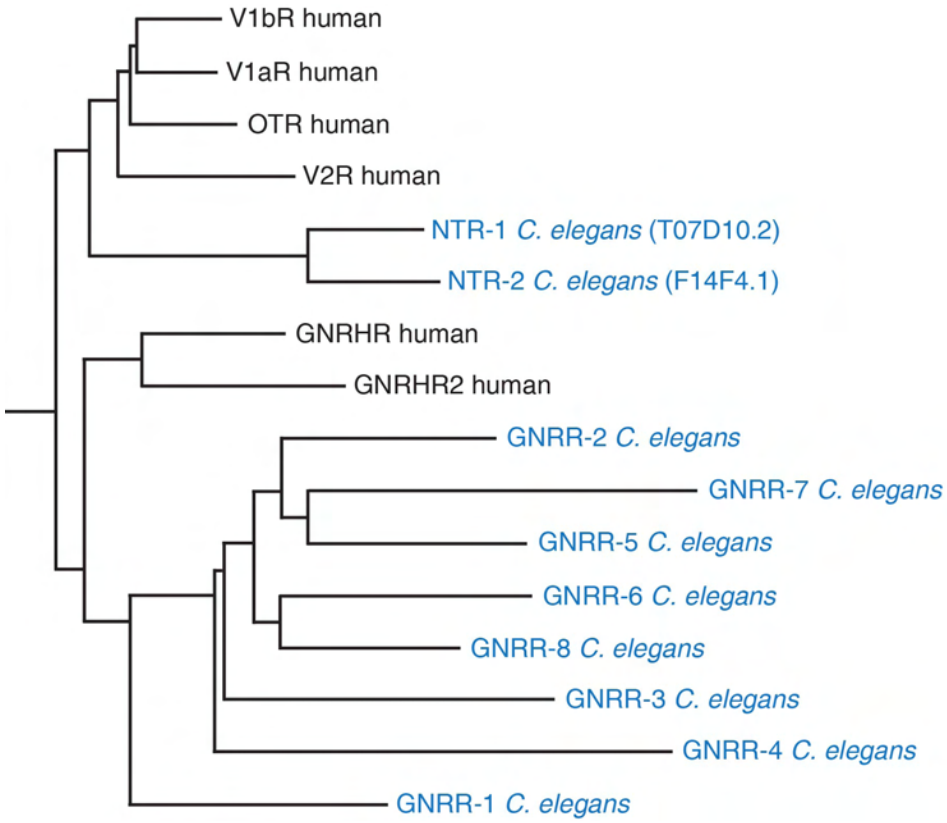

Fig. S4. Phylogenetic analysis of vasopressin and oxytocin receptors. Branch length is proportional to evolutionary distance. The diagram was constructed using TreeFam (www.treefam.org). V1aR, Vasopressin 1a receptor; V1bR, Vasopressin 1b receptor; OTR, Oxytocin receptor; V2R, Vasopressin 2 receptor; GNRHR, Gonadotropin-releasing hormone receptor; GNRR, Gonadotropin-releasing hormone receptor related. Accession numbers of sequences used in the alignment: NP_000697.1 (V1aR), NP_000698.1 (V1bR), NP_000045.1 (V2R), NP_000907.2 (OTR), NP_493193.1 (NTR-1), NP_510477.1 (NTR-2), NP_491453.1 (GNRR-1), NP_506566.1 (GNRR-2), NP_509685.2 (GNRR-3), NP_001024452.1 (GNRR-4), NP_504228.2 (GNRR-5), NP_509865.1 (GNRR-6), NP_509866.2 (GNRR-7), NP_502887.1 (GNRR-8).

Supplementary Fig. S5

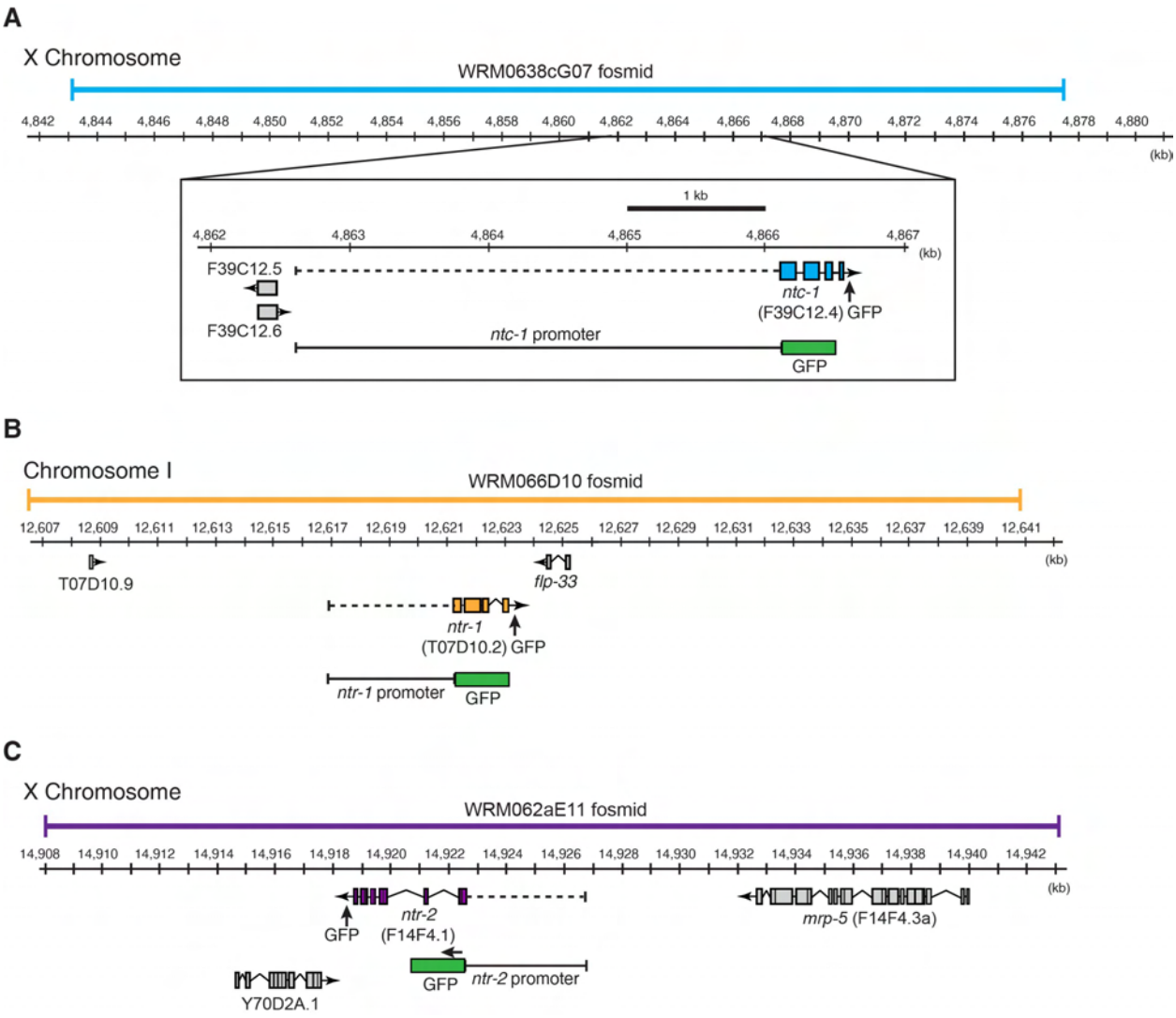

Fig. S5. Genomic regions surrounding *ntc-1*, *ntr-1*, *and ntr-2* and structure of rescuing transgenes, GFP reporter genes, and recombineered fosmid reporter genes. (**A**) Region surrounding *ntc-1* (blue). (**B**) Region surrounding *ntr-1* (orange). (**C**) Region surrounding *ntr-2* (purple). Promoter regions used for GFP fusions are indicated by stopped black bars (~ 4 kb each). For transgenic rescue, the same promoter region (dotted line) was used to drive expression of cDNA linked to GFP via a bicistronic fusion with the SL2 splice leader. For fosmid recombineering, GFP was inserted at the end of the coding region of the gene (arrows) within the illustrated fosmid.

Supplementary Fig. S6

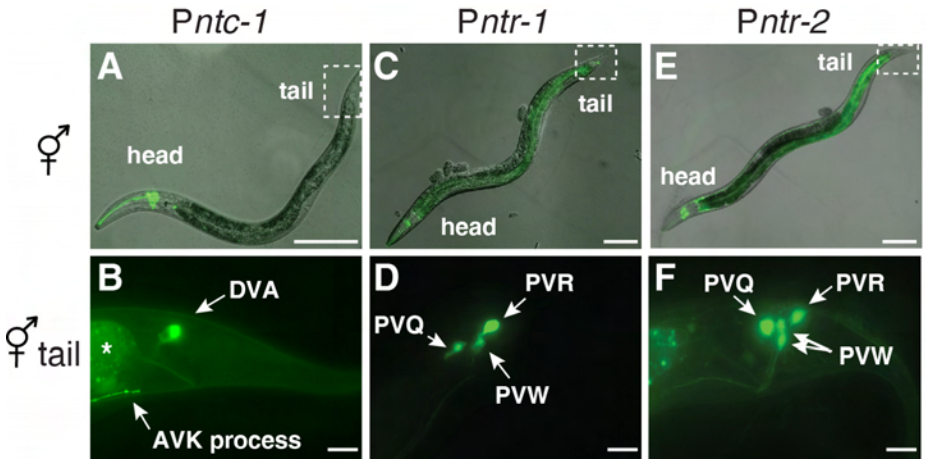

Fig. S6. Expression of *ntc-1*, *ntr-1*, and *ntr-2* reporter genes in hermaphrodites (see Table S1). Upper panels are epifluorescence images overlaid with DIC (differential interference contrast) images, lower panels are labeled epifluorescence images. **A**, **C**, and **E** show expression in adult hermaphrodites; **B**, **D**, and **F** are magnified images of hermaphrodite tails. (**A** and **B**) GFP reporter driven by P*ntc-1*. (**C** and **D**) GFP reporter driven by P*ntr-1*. (**E** and **F**) GFP reporter driven by P*ntr-2*. Asterisks mark autofluorescence; scale bars represent 100 μm in top panels and 10 μm in bottom panels.

Supplementary Fig. S7

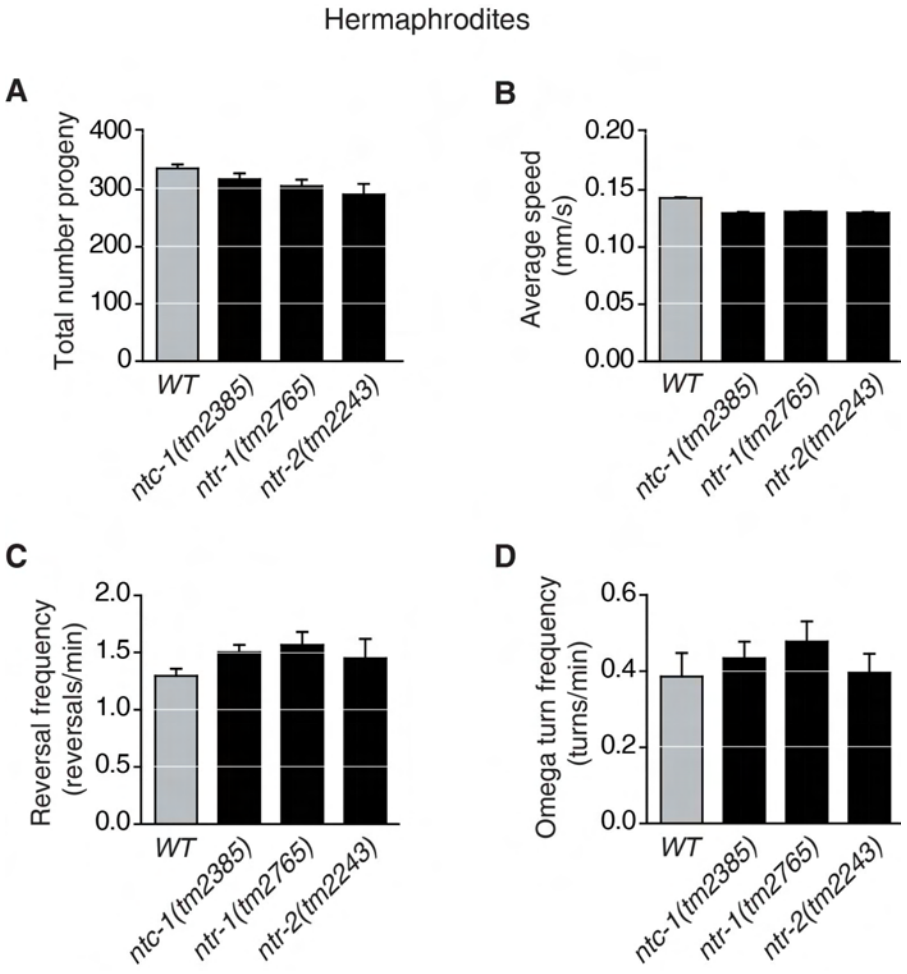

Fig. S7. Hermaphrodites lacking *ntc-1* or its receptors have normal brood size and locomotion on food. (**A**) Total progeny produced by a hermaphrodite over the lifetime of the animal. n = 8-10 animals per data point; error bars represent s.e.m. (**B** to **D**) Locomotion speed, reversal and turning rates of hermaphrodites on food. (**B**) Average speed. (**C**) Average reversal frequency. (**D**) Average omega turn frequency. Movies were recorded for 15 minutes and analyzed using Matlab software as described in Supplementary Methods; speed was analyzed in 5 second bins, reversal and turning frequencies were analyzed in 15 sec bins. Each bar represents a minimum of six separate experiments (20 animals/experiment) conducted on at least two different days. Error bars indicate s.d.

Supplementary Fig. S8

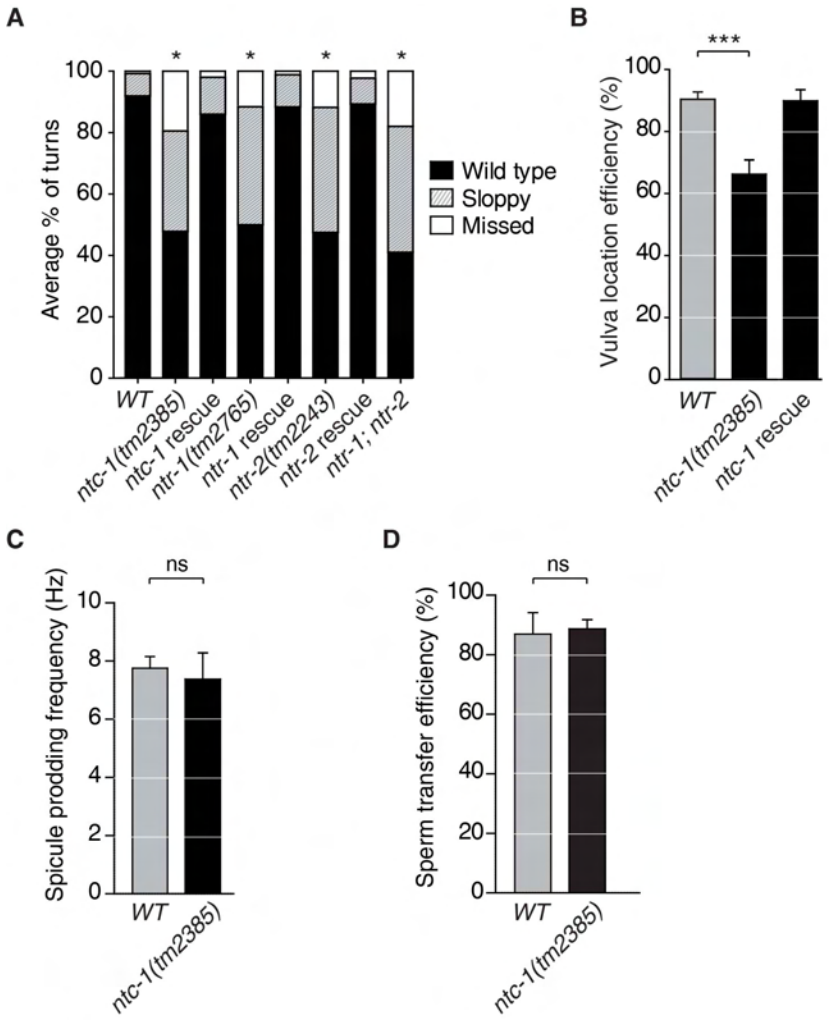

Fig. S8. Male behavior during mating. When a male's tail comes into contact with a hermaphrodite's body he stops moving forward, presses his tail against the hermaphrodite, and backs up along her body in search of the vulva (see Fig. 3A in main text). If he reaches the end of the hermaphrodite's body before encountering the vulva, the male executes a sharp ventral turn while maintaining contact with the hermaphrodite. Once he locates the vulva, he prods the vulva slit with copulatory structures called spicules, then inserts the spicules and transfers sperm. (**A**) Turn quality as represented by the average percentage of turns that were missed (white), sloppy (shaded), or wild-type (black)(*11*). During wild-type turns, the male tail continuously contacts the hermaphrodite body throughout the turn and continues backing along the opposite side after the turn is completed. Sloppy turns are those where the male's tail temporarily loses contact with the hermaphrodite or turns that occur early (before reaching the end of the

hermaphrodite). Missed turns occur when the male's tail completely loses contact with the hermaphrodite's body and the male must move forward before making another attempt at turning. The percentage of each type of turn was determined for individual males and averaged by the total number of males assayed. This normalization corrects for the fact that the total number of turns scored per male varied (see Fig. 3E in main text). Analysis by ANOVA revealed two statistically significant groups; columns marked with asterisks (*) are not significantly different from each other; likewise, unmarked columns are not significantly different from one other. (**B**) Vulva location ability for individual males was calculated as the number of positive vulva detections divided by the total number of vulva encounters while mating. Vulva location efficiency indicates the average behavior of each genotype (n = 39 - 106 males per genotype). (**C**) Spicule prodding frequencies of males during mating (n = 4 males per genotype), measured as described (*13*). Briefly, movies of mating behavior were recorded at 10X with the camera focused on the vulva. To quantify the spicule prodding frequency movies were played back at reduced speed and spicule downstrokes made in 1 s were counted manually. Because the male tail occasionally shifted out of focus only periods of focused spicule movement were counted. (**D**) Sperm transfer efficiency was measured by tracking GFP-histone labeled male sperm that migrated to the spermatheca in a wild-type unlabeled hermaphrodite after mating (n = 22 males per genotype), as described (*34*). Briefly, a single histone-GFP labeled male (wild type or *ntc-1*) was allowed to mate with four unlabeled wild type young adult hermaphrodites on a 5 mm OP50 lawn at 20 °C. After 24 h, hermaphrodite worms were anesthetized with 10 mM NaN3 in M9 buffer for 5 min, mounted onto a 2% agarose pad, and examined using a Zeiss Axioplan2 microscope for the presence of GFP-labeled sperm. ***$P <$ 0.0001 ANOVA with Mann-Whitney test; error bars indicate s.e.m. ns, not significant.

Supplementary Fig. S9

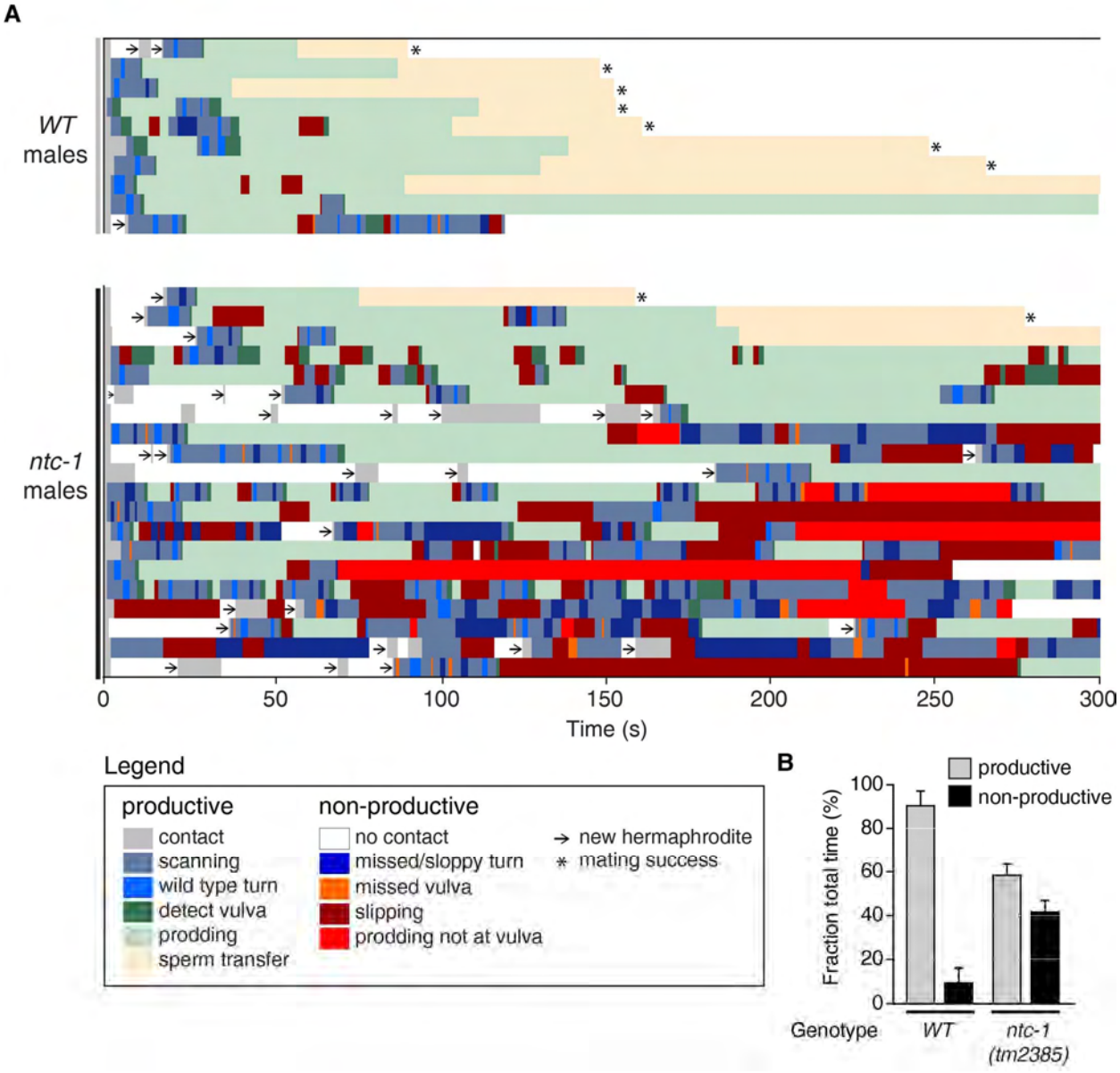

Fig. S9. (**A**) Ethograms of male mating behavior during five-minute mating assays. Mating behavior was recorded at 2 fps using a digital camera (DinoLite Pro AM413T) at a resolution of 245 pixels/mm. Videos were scored manually and Figure was made using Matlab. See Fig. 3G for quantitation of behavioral transitions. (**B**) Fraction of total time that males spent in normal mating behaviors (termed 'productive') and behaviors that disrupted the mating sequence (termed 'non-productive') during the five-minute mating assays. Productive behaviors include contact, scanning, wild type turning, detecting the vulva, prodding, and sperm transfer. Non-productive behaviors include missed or sloppy turning, missing the vulva, slipping, prodding not at the vulva, and losing contact with a hermaphrodite. Slipping refers to loss of contact with the vulva or repetitive backing. n = 10 wild type and n = 20 *ntc-1* males.

Supplementary Fig. S10

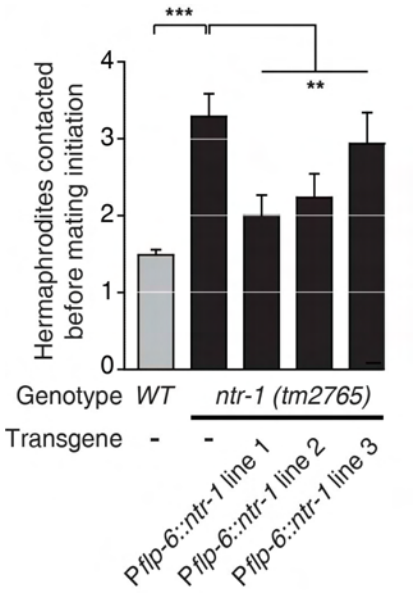

Fig. S10. Response to hermaphrodite contact is partially rescued by expressing an *ntr-1* cDNA under a *flp-6* promoter. The mean number of hermaphrodites that a male's tail contacted before he initiated mating is shown for three independent P*flp-6::ntr-1* transgenic strains. The *flp-6* promoter fragment used for rescue was expressed in the ASE, AWC, AFD, FLP, BAG and SAAD head neurons and in male sensory ray neurons R2B, R5B, R6B and R7B. The only known overlap between *ntr-1*-expressing and *flp-6*-expressing cells is in the ray neurons. $^{**}P < 0.001$; $^{***}P < 0.0001$.

Supplementary Fig. S11

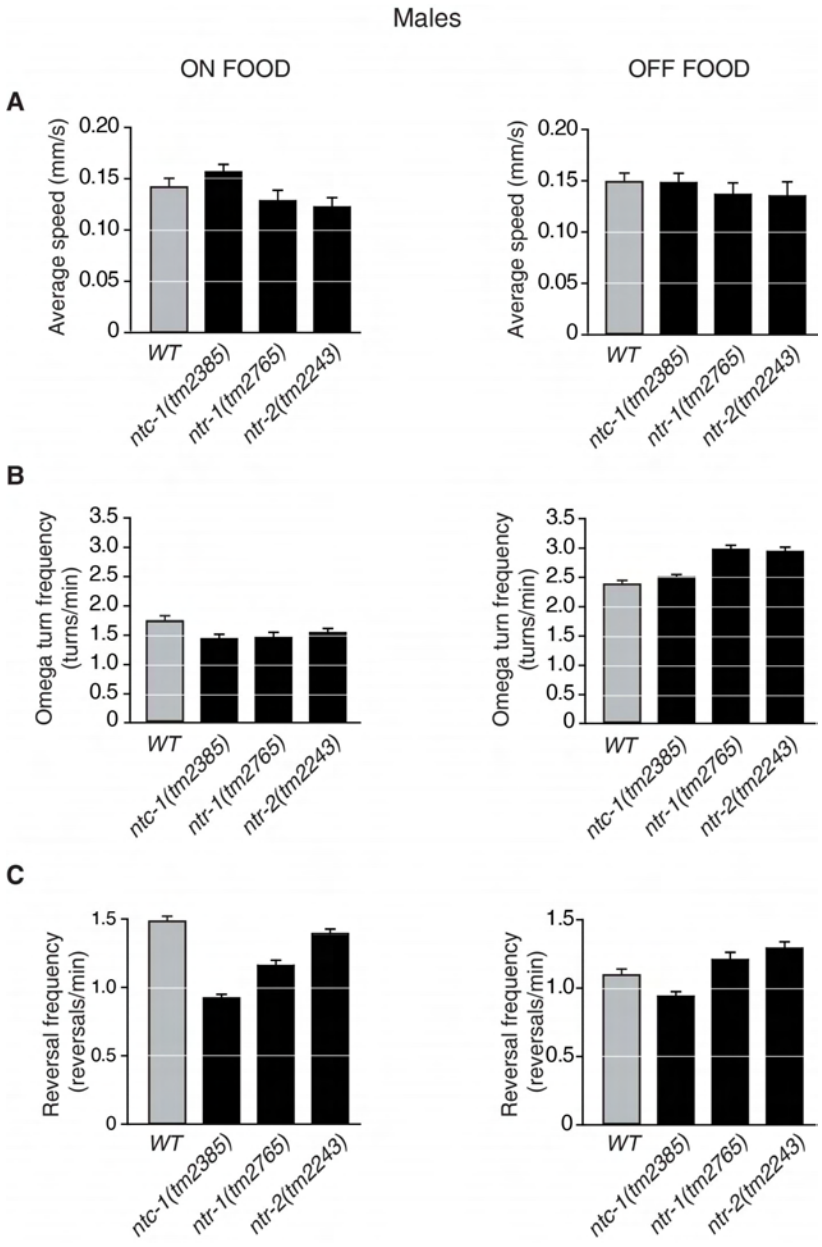

Fig. S11. Males lacking *ntc-1* or its receptors have near-normal locomotion parameters in the presence (left panels) and absence (right panels) of food. (**A**) Average locomotion speed. (**B**) Average omega turn frequency. (**C**) Average reversal frequency. Movies were recorded for 15 minutes and analyzed using Matlab software as described in Supplementary Methods; speed was analyzed in 5 second bins, reversal and turning frequencies were analyzed in 15 sec bins. Each bar represents a minimum of six separate experiments (20 animals/experiment) conducted on at least two different days. Error bars indicate s.d.

Supplementary Fig. S12

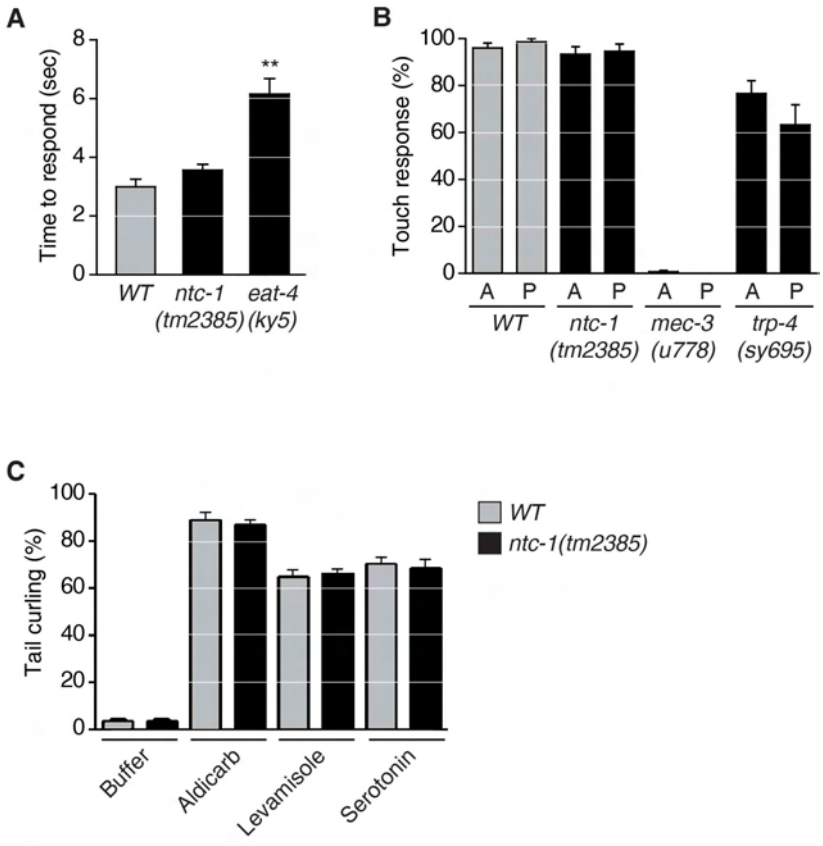

Fig. S12. Males mutant for *ntc-1* have normal responses to aversive chemical and mechanical stimuli, and normal motor responses. (**A**) Time to reversal in response to dilute octanol for males off food (*35*). Individual males engaged in forward motion were scored for the number of seconds to initiate a reversal in response to 30% octanol presented in a glass capillary in front of their noses. n = 120 males/genotype tested on at least three different days. *eat-4(ky5)* males were used as negative controls for the assay. (**B**) Avoidance behavior in response to light touch (*36*). Animals were touched ten times (alternating head and tail touches) and given a score for the number of positive responses within 5 sec. Avoidance behavior was quantified as the percentage of trials in which the animals responded to touch with an eyelash by stopping forward motion or initiating a reversal. The mean percentage score is reported for both anterior and posterior touch response. *mec-3(u778)* and *trp-4(sy695)* were used as controls for the assay. n = 65 males/genotype tested on at least three different days. A, anterior (head) touch; P, posterior (tail) touch. (**C**) Male tail curling behavior, scored as described (*11*) with minor modifications. Young adult males were transferred to 96-well round bottom plates (3 worms/well) containing 100 µl of M9 buffer with or without 20 mM serotonin, 5 mM levamisole, or 5 mM aldicarb. Drug stocks were freshly prepared in M9 buffer just prior to starting the assay. After 10 min, each well was observed individually through a dissecting microscope. Individual males with tails curled tightly for ≥ 5 sec were scored as positive. n = 120 (*WT*) and n = 130 (*ntc-1*). For (**B**) and (**C**), each bar represents the mean percentage score. $^{**}P < 0.001$, Bonferroni t-test; error bars indicate s.e.m.

Supplementary Fig. S13

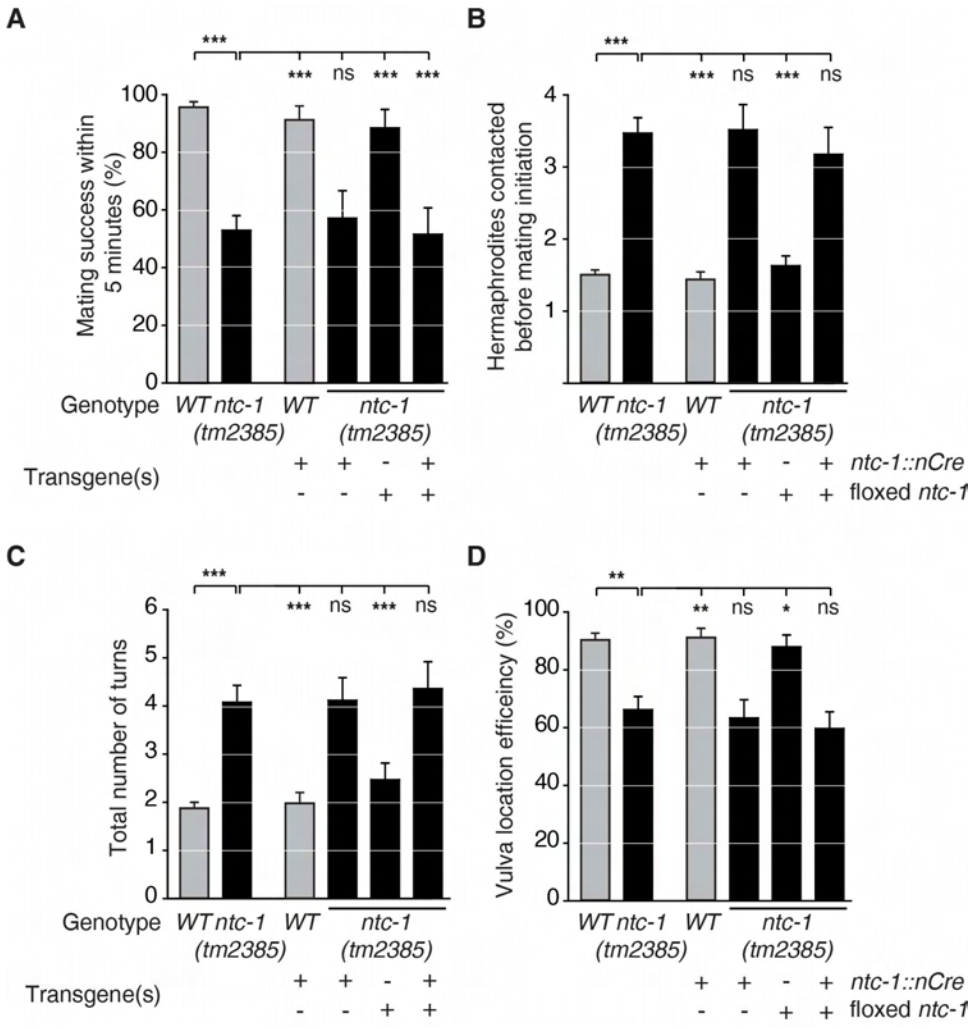

Fig. S13. Inactivation of *ntc-1* in all *ntc-1*-expressing neurons using Cre/*Lox* recombination phenocopies the loss of function *ntc-1* mutant in male mating behavior. (A) Percentage of males that successfully transferred sperm within 5 minutes of first tail contact with a hermaphrodite. (B) Mean number of hermaphrodites that a male's tail contacted before he initiated mating. (C) Mean total number of turns a male executed around a hermaphrodite's body before vulva location. (D) Vulva location ability for individual males, calculated as the number of positive vulva locations divided by the total number of vulva encounters while mating. Vulva location efficiency indicates the average behavior of each genotype. Floxed *ntc-1*, P*ntc-1::LoxP::ntc-1::sl2::gfp::LoxP::mCherry*. $*P < 0.01$, $**P < 0.001$, $***P < 0.0001$ by ANOVA with Dunnett or Mann-Whitney test; error bars indicate s.e.m. Specific Cre-mediated recombination in the DVA mechanosensory neuron with an P*nlp-12::Cre* transgene led to defects only in initial contact response and vulva detection efficiency (see Fig. 4). The restricted effect of DVA inactivation suggests that at least two nematocin-expressing neurons regulate mating: the DVA mechanosensory neuron normally releases nematocin to trigger the response to hermaphrodite contact and vulva detection, but a second site of nematocin release can regulate turning.

Supplementary Fig. S14

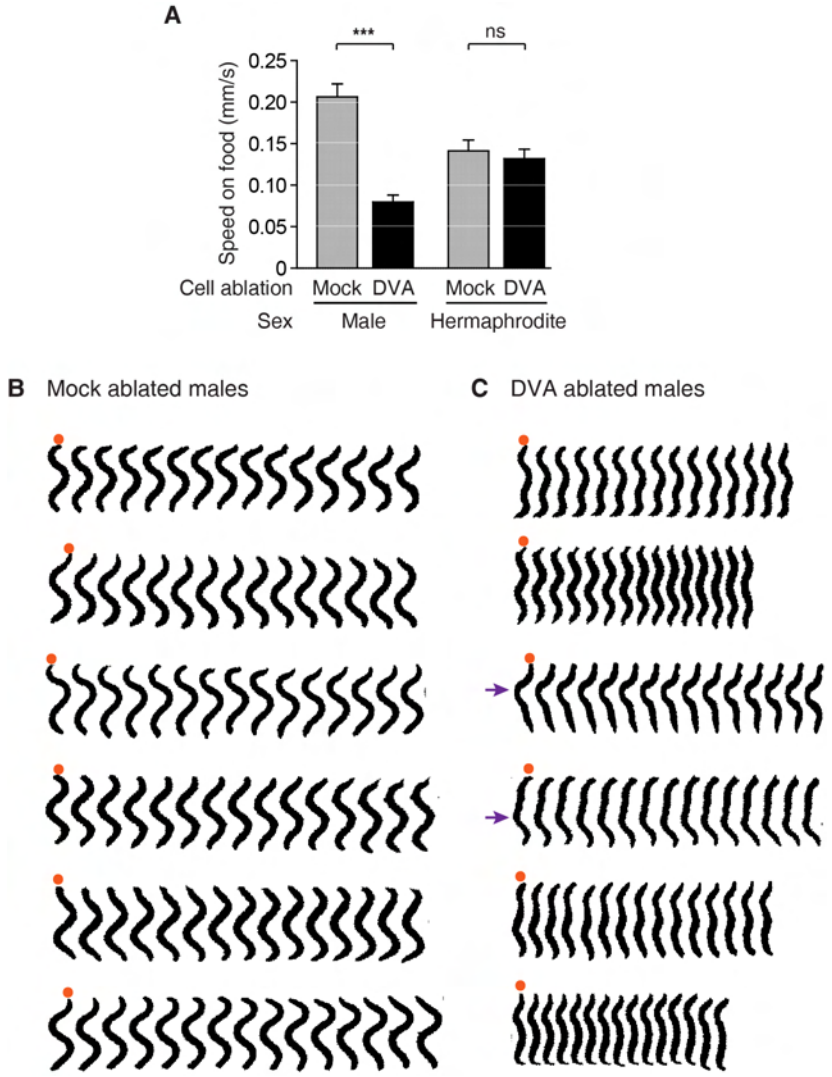

Fig. S14. Laser ablation of DVA leads to abnormal male posture and locomotion. (**A**) Locomotion speed of DVA-ablated and mock-ablated males and hermaphrodites on food. Movies were recorded at 15 fps for 2 minutes; speed was analyzed in 1 s windows. n = 10 animals/genotype; ****P* < 0.0001, Bonferroni t-test; error bars indicate s.e.m. (**B** and **C**) Body posture of DVA-ablated (**B**) and mock-ablated (**C**) males during 1 s (15 frames) of forward movement. Note flatter wave amplitude of DVA-ablated males (all animals) and kinks in the sinusoidal body posture (arrows). Red dot = head. For analysis of shape and locomotion speed, video recordings were made at 15 fps for 2 min on a digital camera (DinoLite Pro AM413T) at a resolution of 245 pixels/mm. Animal body shapes were obtained for each frame by background correction, thresholding, and rotation to align the major axes vertically. Mean forward speed was calculated from successive worm centroid positions during forward locomotion bouts, subject to a 1 s (15 frame) moving window.

Supplementary Table 1

Transgene	Cell (%)
ntc-1p::GFP	AFD (100%), AVK (87%), DVA (83%), NSM (22%), M5 (16%), RIC/AIZ? (16%), D-type motor neurons (33%), VC motor neurons (50%), CPs (20%), PDC (12%)
ntr-1p::GFP	ADL (100%), ADF (100%), ASH (92%), RIC (88%), I2 (59%), PVR (35%), PVQ (72%), PVW (72%), HOB (25%), ray neurons (50%), protractor muscles (31%), intestine (100%), head muscle (6%)
ntr-2p::GFP	ADL (96%), ADF (72%), SMD (96%), RME (66%), AIA (64%), ASH (60%), AVG (56%), RIF (44%), PVS/PVU (17%), SPC (39%), oblique muscles (53%), intestine (90%)
ntr-2::GFP fosmid	PVR (50%), PVQ (58%), PVW (58%), plus neurons as in *ntr-2p::GFP* above.

Table S1. Full expression patterns of transgenes. Cells were identified in *ntc-1p::GFP* (20 hermaphrodites, 22 males); *ntr-1p::GFP* (27 hermaphrodites, 16 males); *ntr-2p::GFP* (25 hermaphrodites, 36 males); and *ntr-2* recombineered fosmid (20 hermaphrodites, 18 males). *ntc-1* and *ntr-1* recombineered fosmid lines had expression patterns similar to *ntc-1p::GFP* and *ntr-1p::GFP*, respectively. Percentages correspond to the fraction of animals examined that expressed GFP in the indicated neurons. Hermaphrodite-specific expression is marked in red and male-specific expression is marked in blue. Immunofluorescent staining with α-NTC-1 antibodies (cross-reactive fraction) showed expression similar to *ntc-1p::GFP* and primarily stained cell bodies; additionally, α-NTC-1 antibodies (cyclized-specific fraction) stained coelemocytes and neuronal processes. α-NTC-1 antibodies did not stain *ntc-1(tm2385)* mutant worms.

References and Notes

1. Z. R. Donaldson, L. J. Young, Oxytocin, vasopressin, and the neurogenetics of sociality. *Science* **322**, 900 (2008). doi:10.1126/science.1158668 Medline

2. D. A. Wagenaar, M. S. Hamilton, T. Huang, W. B. Kristan, K. A. French, A hormone-activated central pattern generator for courtship. *Curr. Biol.* **20**, 487 (2010). doi:10.1016/j.cub.2010.02.027 Medline

3. J. T. Winslow, T. R. Insel, The social deficits of the oxytocin knockout mouse. *Neuropeptides* **36**, 221 (2002). doi:10.1054/npep.2002.0909 Medline

4. M. Kosfeld, M. Heinrichs, P. J. Zak, U. Fischbacher, E. Fehr, Oxytocin increases trust in humans. *Nature* **435**, 673 (2005). doi:10.1038/nature03701 Medline

5. I. D. Neumann, A. H. Veenema, D. I. Beiderbeck, Aggression and anxiety: Social context and neurobiological links. *Front. Behav. Neurosci.* **4**, 12 (2010). Medline

6. Materials and methods are available as supplementary materials on *Science* Online.

7. K. Kim *et al*., Two chemoreceptors mediate developmental effects of dauer pheromone in *C. elegans*. *Science* **326**, 994 (2009). doi:10.1126/science.1176331 Medline

8. J. Hodgkin, Sex determination and dosage compensation in *Caenorhabditis elegans*. *Annu. Rev. Genet.* **21**, 133 (1987). doi:10.1146/annurev.ge.21.120187.001025 Medline

9. I. Mori, Y. Ohshima, Neural regulation of thermotaxis in *Caenorhabditis elegans*. *Nature* **376**, 344 (1995). doi:10.1038/376344a0 Medline

10. W. Li, Z. Feng, P. W. Sternberg, X. Z. Xu, A *C. elegans* stretch receptor neuron revealed by a mechanosensitive TRP channel homologue. *Nature* **440**, 684 (2006). doi:10.1038/nature04538 Medline

11. C. M. Loer, C. J. Kenyon, Serotonin-deficient mutants and male mating behavior in the nematode *Caenorhabditis elegans*. *J. Neurosci.* **13**, 5407 (1993). Medline

12. K. S. Liu, P. W. Sternberg, Sensory regulation of male mating behavior in *Caenorhabditis elegans*. *Neuron* **14**, 79 (1995). doi:10.1016/0896-6273(95)90242-2 Medline

13. L. R. Garcia, P. Mehta, P. W. Sternberg, Regulation of distinct muscle behaviors controls the *C. elegans* male's copulatory spicules during mating. *Cell* **107**, 777 (2001). doi:10.1016/S0092-8674(01)00600-6 Medline

14. Y. Liu *et al*., A cholinergic-regulated circuit coordinates the maintenance and bi-stable states of a sensory-motor behavior during *Caenorhabditis elegans* male copulation. *PLoS Genet.* **7**, e1001326 (2011). doi:10.1371/journal.pgen.1001326 Medline

15. J. Lipton, G. Kleemann, R. Ghosh, R. Lints, S. W. Emmons, Mate searching in *Caenorhabditis elegans*: A genetic model for sex drive in a simple invertebrate. *J. Neurosci.* **24**, 7427 (2004). doi:10.1523/JNEUROSCI.1746-04.2004 Medline

16. T. A. Jarrell *et al*., The connectome of a decision-making neural network. *Science* **337**, 437 (2012). doi:10.1126/science.1221762 Medline

17. H. Ellegren, Sex-chromosome evolution: Recent progress and the influence of male and female heterogamety. *Nat. Rev. Genet.* **12**, 157 (2011). doi:10.1038/nrg2948 Medline

18. E. Z. Macosko *et al*., A hub-and-spoke circuit drives pheromone attraction and social behaviour in *C. elegans*. *Nature* **458**, 1171 (2009). doi:10.1038/nature07886 Medline

19. C. Mello, A. Fire, DNA transformation. *Methods Cell Biol.* **48**, 451 (1995). doi:10.1016/S0091-679X(08)61399-0 Medline

20. D. J. Cline, C. Thorpe, J. P. Schneider, General method for facile intramolecular disulfide formation in synthetic peptides. *Anal. Biochem.* **335**, 168 (2004). doi:10.1016/j.ab.2004.07.015 Medline

21. T. M. Kubiak *et al*., Functional annotation of the putative orphan *Caenorhabditis elegans* G-protein-coupled receptor C10C6.2 as a FLP15 peptide receptor. *J. Biol. Chem.* **278**, 42115 (2003). doi:10.1074/jbc.M304056200 Medline

22. S. H. Chalasani *et al*., Neuropeptide feedback modifies odor-evoked dynamics in *Caenorhabditis elegans* olfactory neurons. *Nat. Neurosci.* **13**, 615 (2010). doi:10.1038/nn.2526 Medline

23. S. J. Husson *et al*., Approaches to identify endogenous peptides in the soil nematode *Caenorhabditis elegans*. *Methods Mol. Biol.* **615**, 29 (2010). doi:10.1007/978-1-60761-535-4_3 Medline

24. B. Tursun, L. Cochella, I. Carrera, O. Hobert, A toolkit and robust pipeline for the generation of fosmid-based reporter genes in *C. elegans*. *PLoS ONE* **4**, e4625 (2009). doi:10.1371/journal.pone.0004625 Medline

25. T. A. Maniar *et al*., UNC-33 (CRMP) and ankyrin organize microtubules and localize kinesin to polarize axon-dendrite sorting. *Nat. Neurosci.* **15**, 48 (2012). doi:10.1038/nn.2970

26. J. Hodgkin, Male phenotypes and mating efficiency in *Caenorhabditis elegans*. *Genetics* **103**, 43 (1983). Medline

27. L. R. Garcia, P. W. Sternberg, *Caenorhabditis elegans* UNC-103 ERG-like potassium channel regulates contractile behaviors of sex muscles in males before and during mating. *J. Neurosci.* **23**, 2696 (2003). Medline

28. M. M. Barr, P. W. Sternberg, A polycystic kidney-disease gene homologue required for male mating behaviour in *C. elegans*. *Nature* **401**, 386 (1999). doi:10.1038/43913 Medline

29. H. Yu, R. F. Pretot, T. R. Burglin, P. W. Sternberg, Distinct roles of transcription factors EGL-46 and DAF-19 in specifying the functionality of a polycystin-expressing sensory neuron necessary for *C. elegans* male vulva location behavior. *Development* **130**, 5217 (2003). doi:10.1242/dev.00678 Medline

30. D. Ramot, B. E. Johnson, T. L. Berry Jr., L. Carnell, M. B. Goodman, The Parallel Worm Tracker: A platform for measuring average speed and drug-induced paralysis in nematodes. *PLoS ONE* **3**, e2208 (2008). doi:10.1371/journal.pone.0002208 Medline

31. S. H. Chalasani *et al*., Dissecting a circuit for olfactory behaviour in *Caenorhabditis elegans*. *Nature* **450**, 63 (2007). doi:10.1038/nature06292 Medline

32. C. I. Bargmann, L. Avery, Laser killing of cells in *Caenorhabditis elegans*. *Methods Cell Biol.* **48**, 225 (1995). doi:10.1016/S0091-679X(08)61390-4 Medline

33. F. M. De Bree, Trafficking of the vasopressin and oxytocin prohormone through the regulated secretory pathway. *J. Neuroendocrinol.* **12**, 589 (2000). doi:10.1046/j.1365-2826.2000.00521.x Medline

34. J. C. Wu *et al*., Sperm development and motility are regulated by PP1 phosphatases in *Caenorhabditis elegans*. *Genetics* **190**, 143 (2012). doi:10.1534/genetics.111.135376 Medline

35. E. R. Troemel, J. H. Chou, N. D. Dwyer, H. A. Colbert, C. I. Bargmann, Divergent seven transmembrane receptors are candidate chemosensory receptors in *C. elegans*. *Cell* **83**, 207 (1995). doi:10.1016/0092-8674(95)90162-0 Medline

36. M. Chalfie, J. Sulston, Developmental genetics of the mechanosensory neurons of *Caenorhabditis elegans*. *Dev. Biol.* **82**, 358 (1981). doi:10.1016/0012-1606(81)90459-0 Medline